



The genetic link between migmatites and granites in Tuyserkhan area (Sanandaj-Sirjan metamorphic belt, western Iran): constraints by mineralogy, geochemistry and thermobarometry

Masoumeh Zare Shooli ¹, Ahmad Ahmadi Khalaji ^{1,*}, Hua-Feng Zhang ², Adel Saki ³

¹ Department of Geology, Faculty of Sciences, Lorestan University, Khorramabad, Iran

² School of Earth Sciences and Resources, China University of Geosciences, Beijing, China

³ Department of Geology, Shahid Chamran University of Ahvaz, Ahvaz, Iran

ARTICLE INFO

Submitted: April 2019

Accepted: November 2019

Available on line: November 2019

* Corresponding author:
ahmadikhalaji.a@lu.ac.ir

DOI: 10.2451/2020PM875

How to cite this article:
Zare Shooli M. et al. (2020)
Period. Mineral. 89, 37-59

ABSTRACT

The metapelitic migmatites and associated granites widely exposed in the Sanandaj-Sirjan metamorphic belt, are natural case to gain insights into the genetic links between the migmatite and associated granite. In Tuyserkhan area, the intrusive of the Alvand batholith invaded the metamorphosed pelitic rocks and resulted in hornfels and migmatites in contact aureoles. Leucosomes and leucocratic granites show substantial variations in trace and major elements. The K₂O and Al₂O₃ contents are high in leucocratic granites. The Na/(Na+Ca) ratios of the leucocratic granites are relatively high in comparison with those of the leucosomes. The SiO₂ content and the constituents of mafic minerals in leucosomes are more than leucocratic granites and show high contents of the Mg/(Mg+Fe) ratio. Leucocratic granites are higher in some HFSE elements (Y, Yb) and leucosomes are higher in the elements that preferably enter plagioclase (Eu). The most important feature of rare earth element patterns is the difference in HFSE amounts between granites and leucosomes. Therefore, the REE pattern of leucosomes and leucocratic granites in Tuyserkhan area depict a lack of a genetic relationship between migmatites and the adjacent granites. Nevertheless, the isotopic age of leucocratic granites, mafic intrusions and migmatites confirm that leucocratic granites were emplaced after the formation of the migmatites. As a result, we proposed that the migmatites formed through contact metamorphism due to the injection of mafic intrusions.

Keywords: Migmatite; partial melting; granite; Tuyserkhan; Sanandaj Sirjan zone; Iran.

INTRODUCTION

The genetic relationships between migmatization and granites have attracted much more interest for several decades (e.g., Fyfe, 1973; White and Chappel, 1977; Vielzeuf and Holloway, 1988; Patino Douce and Harris, 1998; Kriesman, 2001; Corona-Chavez et al., 2006; Lancaster et al., 2009; Toe et al., 2013; Antipin et al., 2018; Zhang et al., 2018; Chen et al., 2015; Xu et al., 2019; Wang et al., 2016). Moreover, leucosome petrogenesis and the importance of deformation and stress in the formation of migmatites were studied by several

researchers (Sawyer and Barnez, 1988; Marchildon and Brown, 2002). Leucosome layers could be generated through subsolidus processes or anatexis (Marchildon and Brown, 2002, 2003). Migmatites provide direct evidences of continental crust partial melting and the composition and distribution of the partial melt might illustrate the migration paths and heterogeneous nature of the host rock. This is because it seems that the rock composition plays an important role in the quantity and composition of the generated melt (Johannes and Gupta, 1982). In most cases, mass balance and textural evidences

show that anatexis is usually preceded by aqueous fluids or the injection of melts (Weber and Barbey, 1986). Partial melting is a proper connective process between metamorphism and magmatism and plays a key role in the spread of migmatites, granulites and S-type granites during crustal development. Granites separated from these rocks (metasedimentary rocks) can become homogeneous and form leucogranites (Chappel and White, 1974; Harris et al., 1995).

Several studies have been carried out on the migmatites from Tuyserkhan (Sepahi, 1999; Baharifar, 2004; Sepahi et al., 2004; Jafari, 2007; Sepahi et al., 2009; Shahbazi et al., 2010; Saki, 2011; Saki et al., 2012; Sepahi et al., 2013; Sepahi et al., 2014; Sepahi et al., 2018). Most studies considered that migmatitization was induced by partial melting due to contact metamorphism triggered by mafic intrusions. However, the genetic relationship between migmatites and neighboring granites has so far not been considered. Sepahi (1999) documented that granitoids were S-type granites produced by partial melting of migmatites. A question is that are migmatites remelting for S-type granite or are aggregations of migmatitic melts for S-type granites? This will be answered in this study.

New data of mineral chemistry and bulk geochemistry, aimed to i) gain new insights on the petrogenetic relationships between the migmatites (the source of leucosomes) and granitic magmas in the Alvand aureoles (western Iran), ii) interpret and explain the leucosome formation through partial melting and/or anatexis, iii) determine possible melt reactions, pressure and temperature estimation and the connection between migmatites and peraluminous granites.

GEOLOGICAL BACKGROUND

The studied area is located in the northwestern Sanandaj-Sirjan geosubstructural zone, western Iran. The Sanandaj-Sirjan Zone in Tuyserkhan area is characterized by the dominance of low- to high-grade regional and contact metamorphic rocks and intrusions (Figure 1). Three tectono-thermal events took place in the Tuyserkhan area: (1) regional metamorphism and deformation related to the Neo-Tethys subduction and (2) the collision of Gondwana continent with Iran micro-continent during late-cretaceous and Early-tertiary eras (Berberian and King, 1981; Alavi, 1994; Mohajjel and Fergusson, 2000; Shahabpour, 2005; Saki, 2010a, 2010b); (3) contact metamorphism resulting by the intrusion of the Alvand batholith into regional metamorphic rocks. The oldest geological units of the area are regional metamorphic rocks belonging to the Paleozoic to Early Jurassic eras (associated with the first tectono-thermal events). The continuation of continental collision and the evolution of orogeny commenced plutonism and the formation of the Alvand batholith (associated

with the second tectono-thermal events). Finally, contact metamorphism, as a result of the intrusion of the Alvand batholith, with a middle Jurassic age (160-150 Ma, Shabazi et al., 2010), into regional metamorphism (Sepahi et al., 2009) (associated with the third tectono-thermal events). Contact metamorphic rocks include spotted schists, hornfelses and migmatites. Metamorphic grade is increased toward the Alvand batholith and a succession of biotite, garnet, andalusite, staurolite, cordierite, K-feldspar and spinel isogrades have been documented (Saki et al., 2012). The studied area includes a group of metamorphic rocks with various metamorphic grades that are invaded by the Alvand plutonic intrusion in middle Jurassic (Shahbazi et al., 2010) (Figure 2). Different parts of this pluton were injected during several phases: first, basic (gabbros) and intermediate (diorites), and then acidic magmas. Shahbazi et al. (2010) reported zircon U-Pb data for the Alvand plutonic rocks: 166.5 ± 1.8 Ma for gabbros, 163.9 ± 0.9 and 161.7 ± 0.6 Ma for granites, and 153.3 ± 2.7 and 154.4 ± 1.3 Ma for leucogranites. Recently, Chiu et al. (2013) and Mahmoudi et al. (2011) revealed that the Alvand granites were formed at about ~ 165 Ma. The rocks from Tuyserkhan area mainly composed by migmatites derived from metapelitic rocks, igneous and metapelitic rocks, with minor metabasaltic (amphibole schist and amphibolite), metacarbonate, and calc-silicate rocks (Saki, 2010; Saki et al., 2012).

FIELD GEOLOGY AND PETROGRAPHY

The migmatite outcrops reported in this paper are situated close to Tuyserkhan. They occur between contact metamorphic rocks (hornfels) and gabbros. Based on field and macroscopic evidences, migmatites in the studied area, using Sawyer et al. (2008) classification scheme, are of metatexite type and display patch, stromatic (or layered), folded and net structures (Figure 3). In the net structure, the haphazardly arranged nodules with different sizes form larger granitic and pegmatitic dykes by joining together of feldspar and quartz portions (Figure 3D).

Tuyserkhan migmatites include leucosome and mesosome portions. The melanosome portion is here absent due to the migration of partial melting leucosomes to other portions of migmatites (Sawyer, 2008).

Mesosomes: Mesosomes are composed by K-feldspar, biotite, andalusite, spinel, cordierite, quartz, plagioclase, garnet and sillimanite minerals. Andalusite is surrounded by spinel + cordierite symplectite in mesosome portions (Figure 4 A,B). Reaction rims of sillimanite are observed around andalusite (Figure 4 C,D). The cordierite has garnet inclusions and the average diameter is almost 2 cm (Figure 4E). There are two types of cordierite in mesosome of migmatites: cordierite-spinel symplectite around andalusite and cordierite porphyroblasts in the

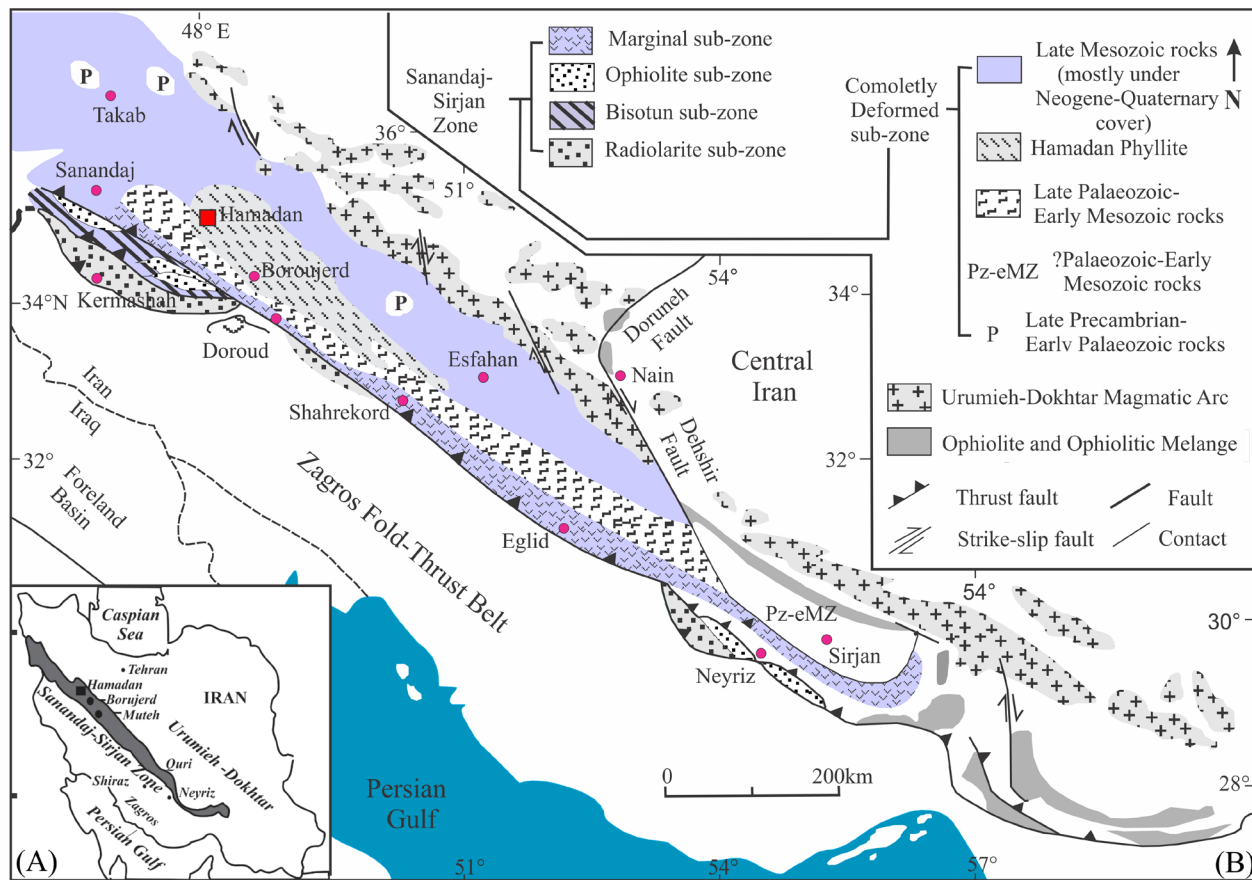


Figure 1. Location of the Sanandaj–Sirjan belt in Iran (A) and tectonic sketch map of the Sanandaj–Sirjan zone in Iran (B; after Mohajjel et al., 2003) and location of the study area that is marked by a red square.

matrix, with inclusions of biotite and garnet (Figure 4E). The average diameter of andalusite in mesosome is approximately 4 cm and has resorbed rims. In the part of mesosome resorbed andalusite is surrounded by spinel-cordierite symplectites. The leucosomes may be seen (quartz, K-feldspar) as patchy in matrix (mesosome) (Figure 4F). K-feldspar forms anhedral grains and shows a micro-perthitic microstructure.

Leucosomes: The leucosomes have granitic composition and magmatic texture. Leucosomes vary in size and range from a few mm to cm in thickness. The leucosome portion contains quartz, K-feldspar and small amounts of garnet and biotite. In leucosomes, K-feldspar is euhedral to subhedral and anhedral, quartz occurs in the areas between them (interstitial texture). Garnet minerals, mm-in-size, are observed in this portion. Quartz and K-feldspar (with microperthite texture) are dominant in this portion that caused the composition of leucosomes is the granitic alkali-feldspar. The minerals in this type of leucosome are K-feldspar (25-45%), quartz (20-35%), biotite (9-15%) and garnet (0-5%). Leucosomes

in Tuyserkan metamorphic aureole are formed due to the partial melting of pelitic rocks.

MACROSCOPIC AND MICROSCOPIC EVIDENCES FOR PARTIAL MELTING

Leucosomes are mainly vein-shaped but rarely spotted. Considering the separate and interrupted nature of these veins it can be concluded that these veins are not related to the igneous intrusions of the area (Figure 5A). Besides, leucosomes and mesosomes are not successively distributed. This characteristic precludes the interpretation of subsolidus segregation for the origin of leucosomes.

The texture of the leucosomes is coarse-grained igneous that is compatible with melt crystallization. Moreover, the grains in leucosomes and melanosomes are contrasting in terms of shape and size. In leucosomes, K-feldspar is euhedral to subhedral while anhedral quartz is found between feldspars (interstitial texture). Additionally, leucosomes show perthitic and myrmekite textures and multiple and Karlsbad twinning are exhibited by plagioclase and feldspar, respectively (Figure 5 B,C,D).

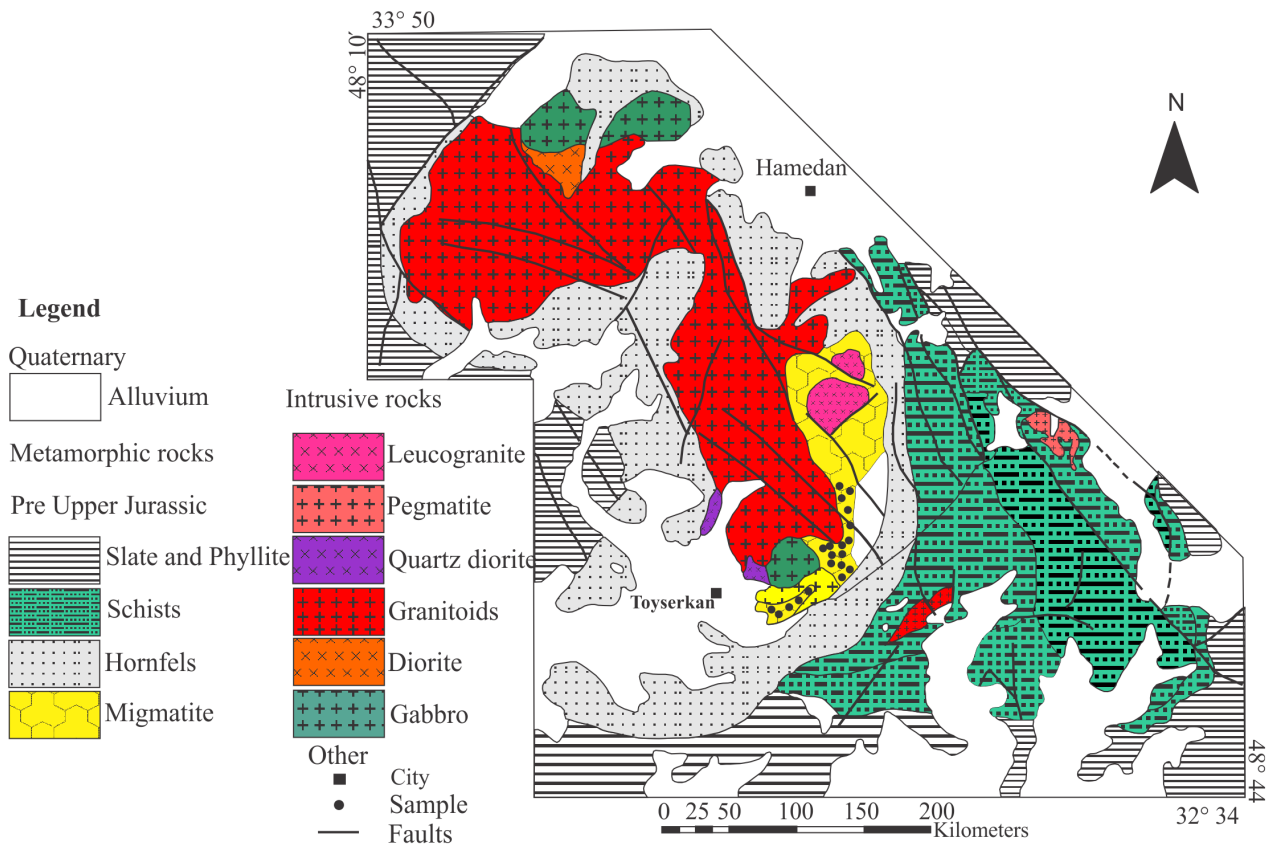


Figure 2. Simplified geological map of Tuyserkan area (modified from Baharifar et al., 2004), with samples locations.

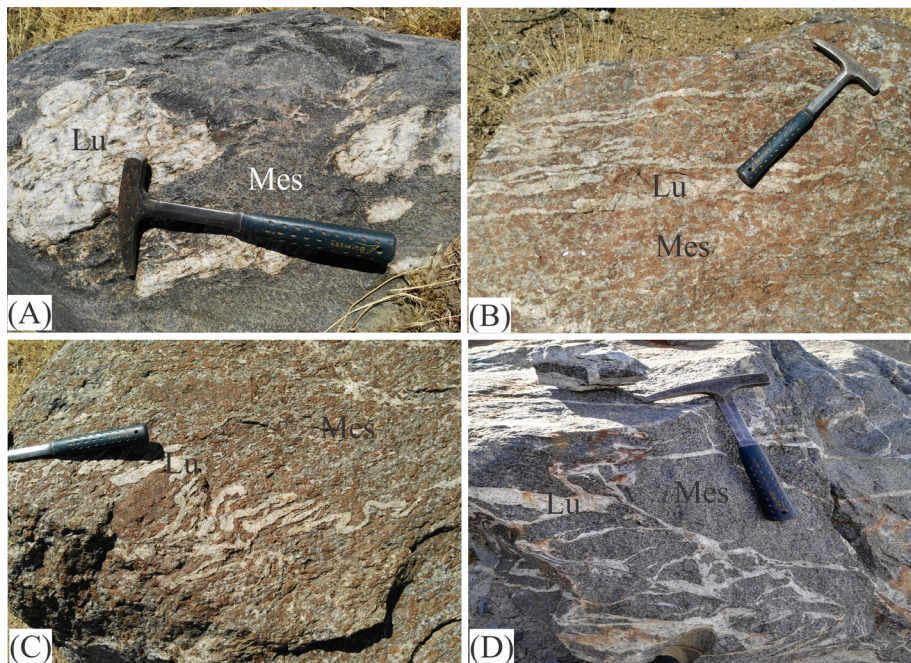


Figure 3. The several existing structures in the migmatites of Tuyserkan area A: patch structure B: stromatic structure C: fold structure D: Net structure.

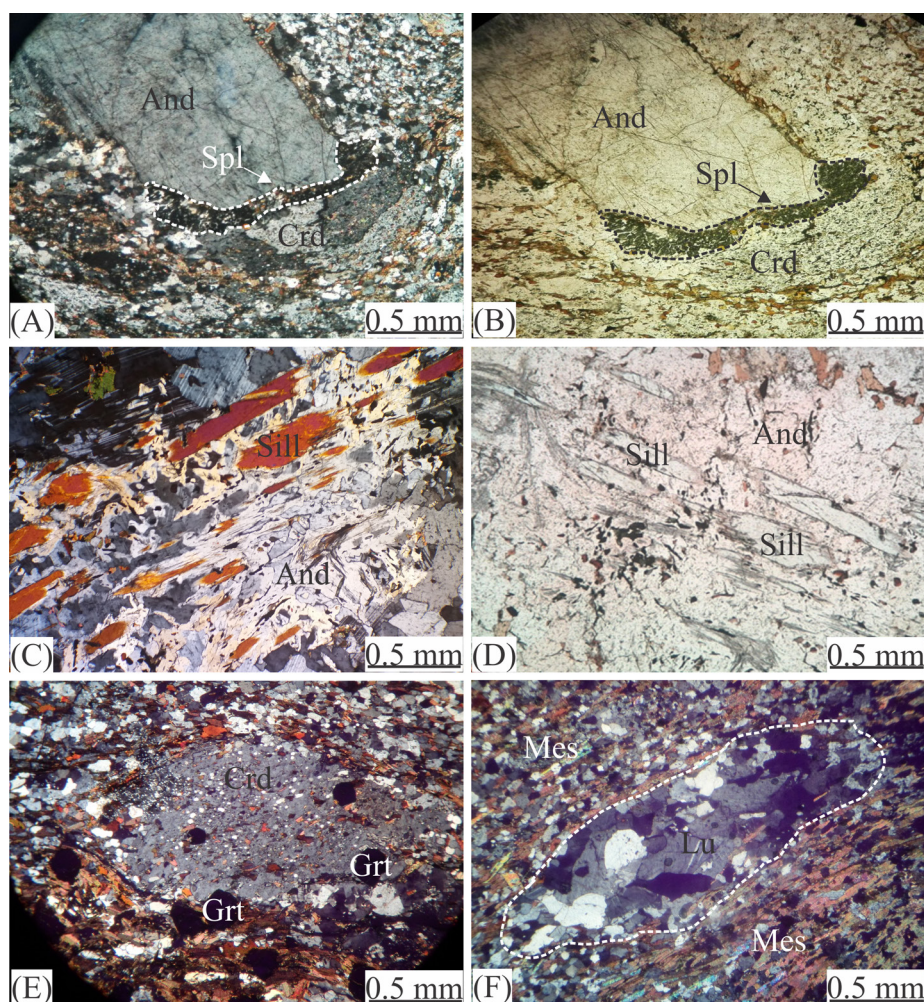


Figure 4. A) Spl+Crd+And symplectite in the mesosome of Tuyskeran migmatites (XPL) B) Spl+Crd+And symplectite in the mesosome of Tuyskeran migmatites (PPL) C) spinel and sillimanite minerals in the mesosome of Tuyskeran migmatites (XPL). D) Spinel and sillimanite minerals in the mesosome of Tuyskeran migmatites (PPL) E) The garnet as inclusion in the cordierite F) Feldspar–plagioclase–quartz patches in the mesosomes of Tuyskeran migmatites.

SAMPLING AND METHODS

Mineral compositions were carried out by electron microprobe (JEOL instrument-JXA 8230) at School of Geosciences and Technology, Southwest Petroleum University, Chengdu, China. This instrument works in wavelength dispersive mode using 15 kv accelerating voltage, 10 nA probe current and 3 to 4 minutes of analytical time for each point. The natural reference materials from the international reference materials provider, the SPI Supplies are applied to calibrate the element intensity, including albite ($\text{NaAlSi}_3\text{O}_8$) for Na and Al, diopside ($\text{MgCaSi}_2\text{O}_6$) for Ca and Si, olivine [$\text{(Mg,Fe)}_2\text{SiO}_4$] for Mg and Fe, Orthoclase (KAlSi_3O_8) for K, bustamite ($\text{CaMnSi}_2\text{O}_6$) for Mn, and rutile (TiO_2) for Ti. The analytical accuracy was about $\pm\% 1$. Representative chemical data for each mineral are shown in Table 1. Details about activities and reactions

considered in the calculations in the KFMASH system by THERMOCALC are in Table 2.

Whole rock major and trace element compositions were determined by XRF (the relative analytical precision was better than 5%) and inductively coupled plasma-mass spectrometry (ICP-MS), respectively (Aushi chemical analysis company, Guangzhou of China). The results are listed in Tables 3 to 5. Before analyzing, rock samples were trimmed to remove the altered surfaces and fresh portions were chipped and powdered with an agate mill to about 200 mesh for major and trace elements analysis. For trace elements analysis, samples were digested with a modified Aqua Regia solution of equal parts concentrated HCl, HNO_3 and DI H_2O for one hour in a heating block or hot water bath. Samples were made up to volume with dilute HCl, then sample splits of 0.5 g, 15 g or 30 g were analyzed.

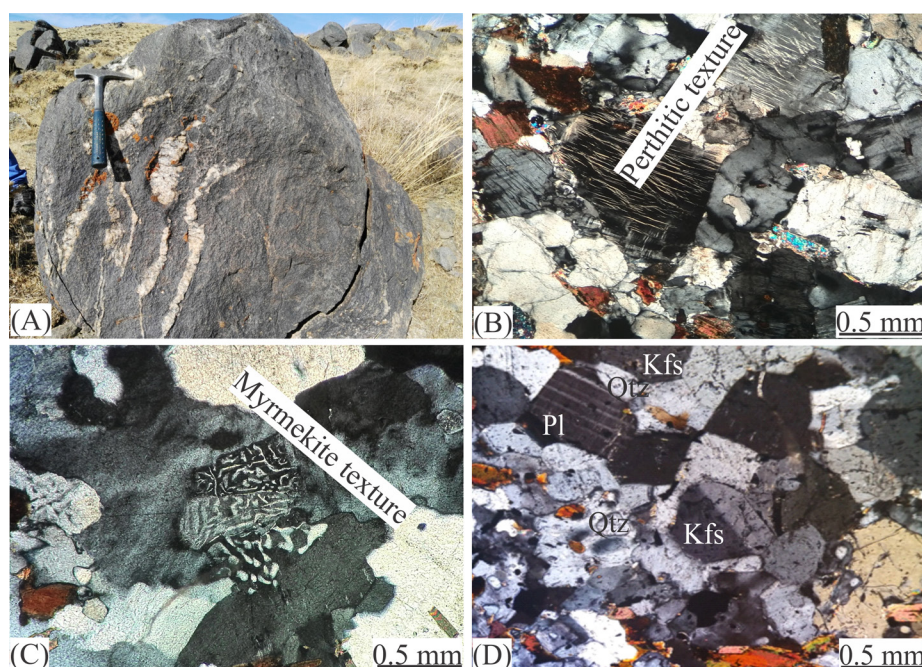


Figure 5. A) Macroscopic evidences for partial melting; B, C, D) Microscopic evidences for partial melting.

RESULTS

Mineral chemistry

Alkali feldspars are untwined and represent intergrowth with plagioclase and quartz (perthite and graphic textures). The grain size of the K-feldspars changes significantly from a few millimeters to several centimeters. The largest K-feldspars are observed in the part of leucosomes of migmatites while the smallest feldspars are in the mesosome or as interstitial grains in coarse grained leucosomes. The chemical analysis of the alkali feldspars of migmatites mesosome is presented in Table 1. Feldspars in migmatites mesosome are high in K and orthoclase end-member. The X_K content of feldspars varies between 0.80 and 0.86.

Plagioclase is present in the part of leucosome and mesosome of migmatites. The chemical analysis of the plagioclase of migmatites mesosome is presented in Table 1. The chemical composition of plagioclase in migmatites mesosome ranges from oligoclase to andesine ($X_{ab}=0.59-0.72$).

Biotite occurs as interstitial grains in the quartz-feldspar matrix and as inclusions in the cordierite. The chemical composition of this mineral is presented in Table 1. Phlogopite-annite is the dominant constituent in the biotite. In migmatites mesosome, all analyzed biotites have $X_{Mg}=0.32$.

The chemical analysis of garnet samples (mesosome) are presented in Table 1. Generally, garnet is high in Fe or almandine. Molar fraction of Fe (X_{Fe}) is between 0.78-

0.80. Garnet lacks Ti or it is too small to be considered.

The chemical characteristics of cordierite is reported in Table 1. Cordierite is high in Fe in the migmatites mesosome. All analyzed cordierites have $X_{Fe}=0.68$.

The spinel chemical composition in the migmatites mesosome is listed in Table 1. It is generally high in Fe or is hercynite, almost all analyzed spinels have $X_{Fe}=0.91$.

Geochemical data (major and trace element compositions)

Major and trace element (including REE) concentrations are listed in Table 3. Leucosomes are characteristically rich in SiO_2 (70.68-77.99 wt%) whereas melanosomes have lower contents of this oxide (56.10-60.57 wt%). Mesosomes have more Al_2O_3 , Fe_2O_3 , MgO, TiO_2 and about CaO amounts which are lower in leucosomes being consistent with the scarcity of Fe-Mg minerals. Generally, leucosomes are enriched in K_2O and SiO_2 while Fe_2O_3 , MgO and TiO_2 are depleted. A/CNK ratios greater than 1, low amounts CaO and peraluminous nature are the features of leucosomes (Figure 6A) that are typical of S-type granites (Figure 6B) (Clemens, 2003). Thus, the S-type characteristic of leucosomes could be the reason for partial melting of migmatites (Droop and Moazzen, 2007).

Another important factor is related to Ba, Rb and Sr. The partial melts produced in the presence of aqueous fluid have low Rb/Sr (0.7-1.6) and high Sr/Ba. This is because restites are depleted in feldspars. This kind of melt shows strongly positive Eu anomaly. However,

Table 1. Representative minerals analyses from mesosome of the Tuyserkan migmatites.

Mineral	Crd	Crd	Crd	Crd	Crd	Grt						
SiO ₂	47.32	46.02	46.15	46.17	46.19	36.15	36.14	36.32	35.81	35.95	36.21	36.00
TiO ₂	0.00	0.00	0.04	0.00	0.02	0.03	0.10	0.00	0.02	0.02	0.05	0.02
Al ₂ O ₃	32.68	31.66	31.61	31.53	31.92	20.79	20.73	20.64	20.53	20.77	20.56	20.67
FeO	14.78	14.63	15.19	14.98	14.83	36.74	36.72	37.00	37.09	36.88	37.10	36.94
MnO	0.44	0.46	0.44	0.47	0.54	3.80	3.57	3.28	3.31	3.45	3.43	3.50
MgO	4.43	4.28	4.32	4.38	4.50	2.39	2.46	2.47	2.55	2.58	2.56	2.62
CaO	0.02	0.04	0.02	0.02	0.03	0.89	0.86	0.91	0.86	0.87	0.91	0.89
Na ₂ O	0.07	0.14	0.10	0.11	0.12	0.00	0.02	0.02	0.01	0.01	0.01	0.00
K ₂ O	0.01	0.01	0.00	0.00	0.00	0.00	0.00	0.00	0.00	0.00	0.01	0.02
Total	99.74	97.25	97.87	97.65	98.15	100.80	100.59	100.64	100.18	100.53	100.84	100.65
Si	4.94	4.93	4.92	4.93	4.90	2.92	2.92	2.93	2.91	2.90	2.92	2.91
Ti	0.00	0.00	0.00	0.00	0.00	0.00	0.01	0.00	0.00	0.00	0.00	0.00
Al	4.02	3.10	3.97	3.97	3.99	1.98	1.98	1.97	1.96	1.98	1.95	1.97
Fe ³⁺	0.11	0.17	0.20	0.20	0.23	0.19	0.18	0.17	0.22	0.21	0.21	0.22
Fe ²⁺	1.18	1.40	1.54	1.14	1.09	2.30	2.31	2.33	2.29	2.28	2.30	2.27
Mn	0.04	0.04	0.04	0.04	0.05	0.26	0.24	0.22	0.23	0.24	0.23	0.24
Mg	0.69	0.68	0.69	0.70	0.71	0.29	0.30	0.30	0.31	0.31	0.31	0.32
Ca	0.00	0.01	0.00	0.00	0.00	0.08	0.07	0.08	0.08	0.08	0.08	0.08
Na	0.01	0.03	0.02	0.02	0.03	0.00	0.00	0.00	0.00	0.00	0.00	0.00
K	0.00	0.00	0.00	0.00	0.00	0.00	0.00	0.00	0.00	0.00	0.00	0.00
	10.99	10.36	11.38	11.00	11.00	8.02	8.01	8.00	8.00	8.00	8.00	8.01
X _{Fe}	0.62	0.66	0.68	0.61	0.50							
X _{Mg}	0.36	0.32	0.30	0.37	0.38							
X _{alm}						0.78	0.79	0.8	0.79	0.78	0.79	0.78
X _{spss}						0.09	0.08	0.08	0.08	0.08	0.08	0.08
X _{py}						0.1	0.1	0.1	0.1	0.11	0.11	0.11
X _{grs}						0.03	0.02	0.03	0.03	0.03	0.03	0.03

the melts produced by OH-bearing minerals like biotite (fluid-absent melting) have higher Rb/Sr ratios (2-6) and lower Sr/Ba ratios and negative Eu anomalies (Harris and Inger, 1992). The parameters mentioned in Table 3 show that in leucosomes Rb/Sr ratio is lower than 2 and Eu has a positive anomaly. These characteristics are representative of fluid-present partial melting source for leucosomes. This fluid could be provided by the adjacent intrusion (Kalsbeek et al., 2001). Leucosomes have very high amounts of Ba that implies feldspar accumulation and shows that these leucosomes are formed due to the crystallization of feldspar and quartz along melt migration paths. This fact is consistent with the high amounts of orthoclase in these leucosomes. Structural relationships and the REE patterns of leucosomes preclude subsolidus differentiation interpretation which is proposed to leucosomes with similar REE patterns (eg. Sawyer and Barnes, 1988; Whitney and Irving, 1994; Zuluaga et al., 2017). Thus, leucosomes are the remnants of a melt phase that are produced by a fluid-present melting reaction. This interpretation is consistent with the similar major element

compositions of these leucosomes and minimum melt compositions (Figure 8B). Besides, the Zr/Hf, and Nb/Ta ratios in leucosomes fall beneath the average continental crust line (Figure 7A,B). The positive correlation between Ba and Eu_N in leucosome samples (Figure 7C) show that partial melting is the main process in the formation of Tuyserkan migmatites (Xu et al., 2007). Hence, field, petrographic, thermometry and geochemical evidences show partial melting as the origin for migmatization.

Lithologic evidences for leucosomes for partial melting

Quartz and K-feldspar minerals are dominant in leucosomes and Fe-Mg minerals like biotite and garnet are either absent or scarce. In order to identify the lithologic composition of leucosome migmatites of the area the feldspar ternary (Inger and Harris, 1993) and R₁R₂ (De La Roche et al., 1980) diagrams were used (Figure 8 A,B). These diagrams display that leucosome migmatites are dominantly granitic in composition. Leucosome petrographic studies in Tuyserkan aureole show that the lithologic composition of leucosomes is

Table 1. ...Continued

Mineral	Bt	Bt	Bt	Bt	Bt	Kf	Kf	Kf	Kf	Kf	Pl	Pl
SiO ₂	34.77	34.76	33.63	34.60	33.50	63.17	63.75	63.15	63.05	63.28	60.98	61.59
TiO ₂	2.91	2.84	2.61	2.77	2.48	0.03	0.04	0.04	0.00	0.00	0.03	0.01
Al ₂ O ₃	17.92	17.99	17.97	18.62	18.35	20.60	19.64	19.68	20.39	19.46	24.17	24.04
FeO	22.71	22.46	22.84	22.54	23.12	0.01	0.00	0.00	0.04	0.06	0.00	0.00
MnO	0.04	0.10	0.12	0.13	0.02	0.03	0.00	0.00	0.01	0.00	0.02	0.00
MgO	5.89	5.97	6.05	6.05	6.05	0.01	0.00	0.00	0.00	0.00	0.01	0.00
CaO	0.06	0.03	0.02	0.01	0.00	0.06	0.06	0.08	0.04	0.06	6.14	5.64
Na ₂ O	0.11	0.07	0.09	0.08	0.09	1.65	1.57	2.16	1.65	1.68	7.92	8.26
K ₂ O	9.45	9.38	9.27	9.71	9.53	14.32	14.53	13.82	14.34	14.42	0.18	0.19
Total	93.85	93.61	92.61	94.51	93.14	99.87	99.60	98.94	99.51	98.96	99.45	99.73
Si	2.74	2.74	2.70	2.71	2.68	2.91	2.95	2.94	2.92	2.95	2.72	2.74
Ti	0.17	0.17	0.16	0.16	0.15	0.00	0.00	0.00	0.00	0.00	0.00	0.00
Al	1.67	1.67	1.70	1.72	1.73	1.12	1.07	1.08	1.11	1.07	1.27	1.26
Fe ³⁺	0.00	0.00	0.00	0.00	0.00	0.00	0.00	0.00	0.00	0.00	0.00	0.00
Fe ²⁺	1.50	1.48	1.53	1.48	1.54	0.00	0.00	0.00	0.00	0.00	0.00	0.00
Mn	0.00	0.08	0.01	0.01	0.00	0.00	0.00	0.00	0.00	0.00	0.00	0.00
Mg	0.69	0.70	0.72	0.71	0.72	0.00	0.00	0.00	0.00	0.00	0.00	0.00
Ca	0.01	0.00	0.00	0.00	0.00	0.00	0.00	0.00	0.00	0.00	0.29	0.27
Na	0.02	0.01	0.01	0.01	0.01	0.15	0.14	0.20	0.15	0.15	0.69	0.71
K	0.95	0.94	0.95	0.97	0.97	0.84	0.86	0.82	0.85	0.86	0.01	0.01
	7.75	7.79	7.78	7.77	7.80	5.02	5.02	5.04	5.03	5.03	4.98	4.99
X _{Fe}	0.68	0.68	0.68	0.69	0.68							
X _{Mg}	0.32	0.32	0.30	0.32	0.32							
X _K						0.85	0.86	0.8	0.85	0.85		
X _{an}						0.15	0.14	0.19	0.15	0.15	0.7	0.72
Mineral	Pl	Pl	Pl	Pl	Pl	Spl						
SiO ₂	60.00	59.62	59.66	59.55	59.49	0.01	0.00	0.05	0.03	0.00	0.03	0.01
TiO ₂	0.01	0.03	0.00	0.00	0.08	0.08	0.02	0.06	0.00	0.00	0.00	0.00
Al ₂ O ₃	24.68	25.42	25.75	24.72	24.84	54.67	54.77	55.55	54.93	54.90	54.91	54.23
FeO	0.02	0.44	0.12	0.05	0.15	42.30	41.48	41.47	41.89	41.27	41.44	41.59
MnO	0.00	0.02	0.00	0.01	0.00	0.43	0.47	0.35	0.41	0.31	0.44	0.44
MgO	0.00	0.12	0.01	0.00	0.09	1.70	1.75	1.58	1.75	1.80	1.74	1.82
CaO	6.51	7.38	7.67	6.79	7.84	0.00	0.00	0.00	0.00	0.00	0.00	0.00
Na ₂ O	7.92	7.24	7.13	7.81	6.44	0.02	0.03	0.02	0.02	0.04	0.02	0.02
K ₂ O	0.16	0.12	0.10	0.11	0.18	0.00	0.00	0.00	0.00	0.00	0.00	0.00
Total	99.28	100.39	100.42	99.04	99.10	99.20	98.52	99.07	99.04	98.33	98.58	98.11
Si	2.69	2.65	2.65	2.68	2.67	0.00	0.00	0.00	0.00	0.00	0.00	0.00
Ti	0.00	0.00	0.00	0.00	0.00	0.00	0.00	0.00	0.00	0.00	0.00	0.00
Al	1.30	1.33	1.35	1.31	1.32	1.88	1.89	1.91	1.89	1.90	1.90	1.88
Fe ³⁺	0.00	0.02	0.00	0.00	0.01	0.12	0.11	0.09	0.11	0.10	0.10	0.12
Fe ²⁺	0.00	0.00	0.00	0.00	0.00	0.92	0.91	0.92	0.91	0.91	0.91	0.91
Mn	0.00	0.00	0.00	0.00	0.00	0.01	0.01	0.01	0.01	0.01	0.01	0.01
Mg	0.00	0.01	0.00	0.00	0.01	0.07	0.08	0.07	0.80	0.08	0.08	0.08
Ca	0.31	0.35	0.37	0.33	0.38	0.00	0.00	0.00	0.00	0.00	0.00	0.00
Na	0.69	0.62	0.61	0.68	0.56	0.00	0.01	0.00	0.00	0.00	0.00	0.00
K	0.01	0.01	0.01	0.01	0.01	0.00	0.00	0.00	0.00	0.00	0.00	0.00
	5.00	4.99	4.99	5.01	4.96	3.00	3.01	3.00	3.72	3.00	3.00	3.00
X _{Fe}						0.92	0.91	0.92	0.91	0.91	0.91	0.91
X _{an}	0.68	0.63	0.62	0.67	0.59							

Table 2. Activity values used for calculating equilibrium reactions in the KFMASH system by THERMOCALC in Tuyserkan migmatites.

Activity minerals assemblage in Tuyserkan migmatites	Independent set of reactions
H ₂ O, q, and, sp 0.088, herc 0.75, phl 0.0162, ann 0.11, east 0.019, ferd 0.29, crd 0.24, alm 0.42, py 0.0016	(1) 6and + phl + 3alm = 3sp + ann + 3ferd (2) 2and + phl + alm = sp + ann + crd (3) 6and + 2phl + 3alm = 3herc + 2ann + 3crd

Table 3. Major and trace element contents from mesosomes migmatites of Tuyserkan (Mes: mesosome).

Sample	Tu-10	Tu-13	Tu-12	Tu-11	Tu-14	Tu-8	Tu-15	Tu-16	Tu-17	Tu-9	Average
(%wt)	Mes										
SiO ₂	56.10	58.27	63.57	56.79	56.82	59.03	56.16	60.45	59.43	57.19	58.38
TiO ₂	1.12	1.01	0.77	1.02	0.75	0.89	0.94	0.93	1.01	1.07	0.95
Al ₂ O ₃	21.44	20.46	18.64	21.49	21.47	20.01	21.55	20.14	20.32	20.95	20.65
Fe ₂ O ₃	9.11	8.62	7.26	9.28	8.95	7.95	8.43	7.69	8.58	8.87	8.47
Cr ₂ O ₃	0.04	0.04	0.04	0.06	0.06	0.04	0.05	0.03	0.06	0.04	0.05
MnO	0.20	0.20	0.13	0.24	0.22	0.18	0.18	0.16	0.17	0.20	0.19
MgO	2.92	2.76	2.11	2.76	2.98	2.45	2.64	2.48	2.48	2.84	2.64
CaO	0.98	0.85	0.58	0.77	0.62	0.89	0.68	0.77	0.76	0.92	0.78
Na ₂ O	1.70	1.57	1.74	1.58	1.52	1.96	1.66	1.70	1.52	1.64	1.66
K ₂ O	4.19	4.19	3.34	4.31	4.58	5.02	4.86	4.37	4.37	4.19	4.34
P ₂ O ₅	0.15	0.13	0.15	0.11	0.13	0.11	0.14	0.12	0.12	0.14	0.13
Sum	97.95	98.10	98.33	98.41	98.10	98.53	97.29	98.84	98.82	98.05	98.24
(ppm)											
Cr	300	250	260	380	310	290	360	230	390	275	304.5
V	244	218	159	232	164	186	208	199	208	231	204.90
Cs	9.52	10.10	9.34	8.64	10.90	9.94	8.90	8.45	7.47	9.81	9.31
Rb	178.5	193.0	138.5	191.0	198.5	217	192.0	170.5	171.0	185.8	183.6
Sr	123.0	121.5	105.0	121.5	131.0	155.5	130.5	137.0	118.5	122.3	126.6
Ba	380	415	301	423	417	459	424	417	367	398	400
Th	19.00	17.25	13.25	17.75	16.55	15.25	16.40	15.45	16.10	18.13	16.51
U	3.51	3.19	2.85	2.87	3.08	2.82	2.98	2.89	2.87	3.35	3.04
Ta	1.6	1.4	1.0	1.1	1.0	1.1	1.1	1.2	1.2	1.5	1.2
Nb	21.3	19.3	14.3	18.1	15.0	16.8	17.2	16.8	18.2	20.3	17.7
La	51.4	46.9	36.2	49.2	45.3	42.0	45.1	42.5	43.6	49.2	45.1
Ce	105.5	96.1	75.1	101.0	93.6	86.8	92.7	88.9	90.2	100.8	93.1
Pr	11.30	10.20	8.08	10.80	10.00	9.34	10.10	9.33	9.86	10.75	9.98
Nd	42.1	37.8	30.2	40.5	36.8	34.4	37.8	34.7	36.6	40.0	37.1
Sm	7.73	7.28	5.70	7.11	6.89	6.08	7.19	6.17	6.70	7.51	6.84
Eu	1.36	1.42	1.13	1.57	1.31	1.50	1.39	1.44	1.47	1.39	1.40
Gd	7.10	6.67	5.03	5.97	5.55	5.11	6.39	5.52	6.07	6.89	6.03
Tb	0.93	0.89	0.72	0.78	0.75	0.68	0.86	0.76	0.82	0.91	0.81
Dy	5.32	5.11	4.22	4.47	4.32	4.12	5.24	4.69	4.90	5.22	4.76
Ho	1.09	1.02	0.89	0.89	0.85	0.87	1.06	0.95	0.99	1.06	0.97
Er	3.34	3.11	2.82	2.86	2.68	2.79	3.39	2.96	3.20	3.23	3.04
Tm	0.48	0.46	0.40	0.42	0.39	0.41	0.50	0.43	0.43	0.47	0.44
Yb	3.19	3.05	2.77	2.78	2.60	2.79	3.22	2.70	2.94	3.12	2.92
Lu	0.49	0.49	0.42	0.43	0.42	0.46	0.51	0.43	0.47	0.49	0.46
Y	31.3	30.1	26.6	26.1	24.7	25.2	31.6	28.0	28.7	30.7	28.3
Hf	6.3	6.1	5.2	6.0	4.9	5.1	5.9	5.1	5.8	6.2	5.7
Zr	233	222	197	225	182	192	221	185	217	227.5	210.15
Ga	26.6	25.3	21.5	26.5	25.1	23.7	27.3	23.8	24.9	26.0	25.07
Sn	3	3	3	2	3	3	3	2	2	3	2.7
W	11	9	12	16	13	11	16	8	18	10	12.40
Eu*/Eu	2.76	2.29	1.77	2.15	2.02	1.83	2.21	1.92	2.1	2.36	2.12
(La/Yb) _N	1.15	10.45	8.88	12.02	11.84	10.23	9.52	10.69	10.08	10.71	10.49

Table 3... Continued. Major and trace element contents from metapelite of Tuyserkan.

Sample (%wt)	Tu-1 Pelite	Tu-2 Pelite	Tu-3 Pelite	Tu-5 Pelite	Tu-7 Pelite	Tu-8 Pelite	Tu-9 Pelite	Tu-1 Pelite	Tu-4 Pelite	Tu-6 Pelite	average Pelite
SiO ₂	63.06	61.75	64.84	62.66	59.31	60.14	65.26	62.70	59.70	62.30	62.172
TiO ₂	0.79	0.84	0.65	0.83	0.98	0.79	0.78	0.79	0.89	0.88	0.822
Al ₂ O ₃	18.27	19.26	17.98	19.02	20.24	20.12	17.54	18.83	20.18	18.89	19.033
Fe ₂ O ₃	6.44	7.94	7.33	7.13	8.44	7.34	7.02	7.18	7.89	7.73	7.444
Cr ₂ O ₃	0.03	0.03	0.03	0.03	0.05	0.04	0.03	0.04	0.05	0.04	0.037
MnO	0.13	0.14	0.19	0.13	0.16	0.13	0.13	0.13	0.15	0.15	0.144
MgO	1.82	2.31	2.10	1.99	2.55	2.21	1.99	2.10	2.38	2.27	2.172
CaO	0.42	0.37	0.51	0.52	0.71	0.63	0.58	0.60	0.70	0.60	0.564
Na ₂ O	2.04	1.18	1.60	1.62	1.52	1.94	1.74	1.84	1.73	1.63	1.684
K ₂ O	4.3	4.26	3.31	3.90	4.33	3.93	3.22	3.58	4.13	3.78	3.874
P ₂ O ₅	0.18	0.15	0.16	0.17	0.14	0.16	0.17	0.17	0.15	0.16	0.161
LOI	1.95	1.49	1.47	1.97	1.90	2.04	1.81	1.92	1.97	1.83	
Sum	97.48	98.23	98.70	98.00	98.43	97.43	98.46	97.96	97.95	98.43	98.107
(ppm)											
Cr	220	200	210	260	350	270	260	265	310	305	265
V	160	177	144	175	207	193	148	170.5	200	177.5	175.2
Cs	14.65	10.40	15.70	9.48	7.27	10.50	9.70	10.10	8.89	8.49	10.518
Rb	188.5	177.0	158.5	154.5	176.0	162.5	133.0	147.8	169.3	154.5	162.15
Sr	104	65.7	76.1	92.8	115.0	117.5	104.5	111.0	116.3	109.8	101.26
Ba	309	309	245	359	337	354	282	318	346	310	316.8
Th	13.45	14.20	12.45	14.45	15.65	14.05	12.80	13.40	14.90	14.20	13.955
U	2.84	3.00	2.79	3.01	2.72	2.89	2.79	2.80	2.80	2.80	2.844
Ta	1	1.0	0.9	1.1	1.1	1.0	1.0	1.0	1.1	1.1	1.03
Nb	14.1	14.2	12.5	15.3	17.6	15.9	14.7	15.0	17.0	16.0	15.23
La	36.3	39.9	33.6	39.1	43.5	40.0	35.2	37.6	41.8	39.4	38.63
Ce	73.9	82.8	68.2	81.5	88.9	82.3	73.4	77.9	85.6	81.2	79.56
Pr	8.1	8.90	7.48	8.81	9.56	8.93	7.77	8.35	9.25	8.67	8.582
Nd	30.1	33.2	27.9	33.0	35.9	33.6	29.8	31.7	34.8	32.9	32.29
Sm	5.54	5.72	5.05	6.23	6.68	6.12	5.67	5.90	6.40	6.18	5.949
Eu	1.24	1.23	1.02	1.20	1.47	1.37	1.14	1.26	1.42	1.31	1.266
Gd	4.92	5.09	4.75	5.78	5.95	5.51	5.38	5.45	5.73	5.67	5.423
Tb	0.72	0.73	0.66	0.82	0.79	0.81	0.76	0.79	0.80	0.78	0.766
Dy	4.45	4.50	3.93	4.97	4.38	4.61	4.49	4.55	4.50	4.44	4.482
Ho	0.91	0.95	0.80	0.99	0.89	0.93	0.96	0.95	0.91	0.93	0.922
Er	2.85	2.96	2.59	3.04	2.73	3.08	2.98	3.03	2.91	2.86	2.903
Tm	0.43	0.44	0.38	0.46	0.39	0.44	0.44	0.44	0.42	0.42	0.426
Yb	2.81	2.91	2.43	2.94	2.49	2.87	2.73	2.80	2.68	2.61	2.727
Lu	0.43	0.44	0.38	0.48	0.40	0.44	0.42	0.43	0.42	0.41	0.425
Y	25.9	26.8	23.0	28.8	26.3	27.5	27.2	27.4	26.9	26.8	26.66
Hf	5	4.8	4.5	5.6	5.5	4.9	5.4	5.2	5.2	5.5	5.15
Zr	187	175	170	210	207	186	203	194.5	196.5	205	193.4
Ga	20.9	23.3	20.6	22.4	25.0	24.4	19.8	22.1	24.7	22.4	22.56
Sn	4	4	3	4	2	4	8	6	3	5	4.3
W	13	9	9	13	14	14	12	13	14	13	12.4
Eu/*Eu	1.72	1.78	1.62	1.97	2.07	1.9	1.81	1.85	2	1.96	1.87
(La/Yb)N	8.78	9.32	9.39	9.04	11.86	9.47	8.76	9.12	10.59	10.26	9.61

similar to leucocratic to partial melting granites and is consistent with melt-crystallized source. In order to identify the protolith of migmatites different diagrams are used. The plot of the studied samples on A'FK, ACF

(Winkler, 1976) and CNK triangles diagrams show that the protoliths of Tuyserkan migmatites are dominantly pelitic (Figure 8 C,D).



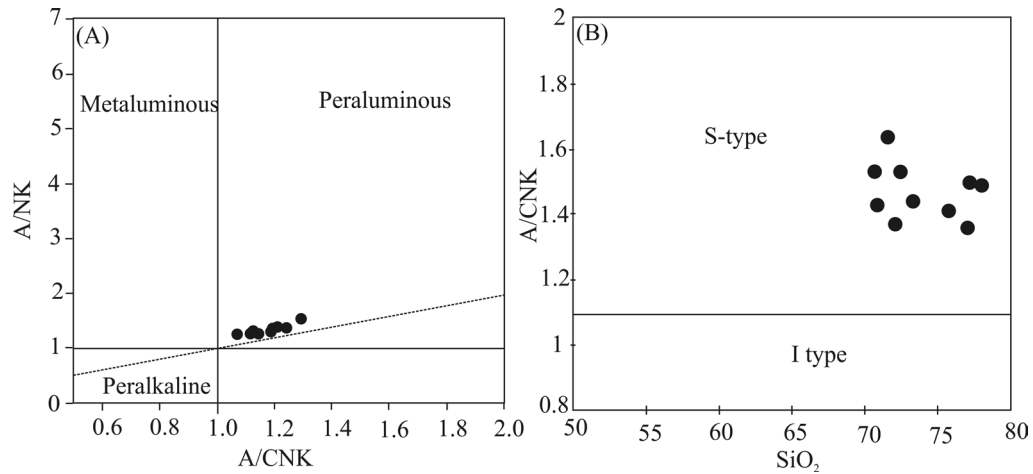


Figure 6. A) A/CNK vs A/NK diagram for migmatite leucosomes from Shand (1943) B) A/CNK vs SiO₂ diagram for migmatite leucosomes from Whalen et al. (2006).

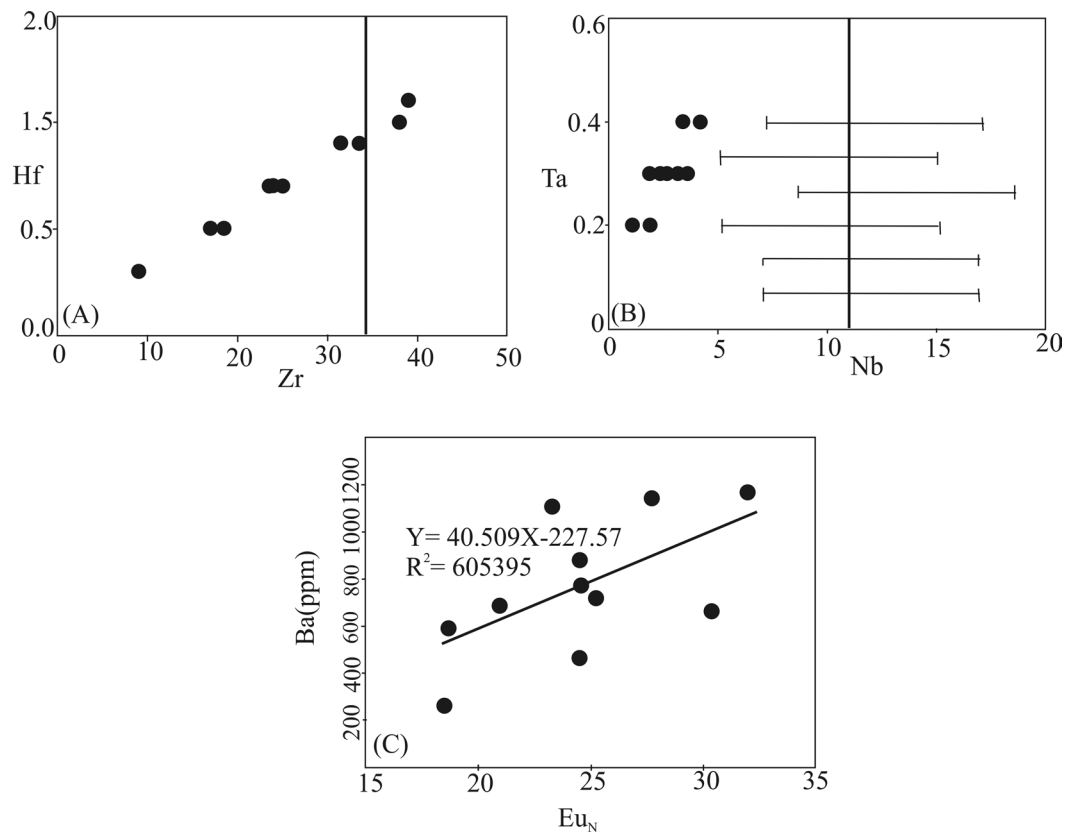


Figure 7. A, B) Zr/ Hf and Nb/ Ta ratios and estimated ratios for upper continental crust (Rudnick, 1995) (Dark index line) C) Anomaly ratio of Eu_N vs Ba.

Thermometry evidence of leucosomes for partial melting

Leucosome temperature calculations based on zircon-saturation thermometer represent the obtained leucosome temperature based on the equation of Watson and Harrison (2005) is 656-766 °C (Samples Tu-11=656, Tu-12=766, Tu-13=731, Tu-14=765, Tu-15=728, Tu-10= 749, Tu-17=

708, Tu-16=754, Tu-8=725, Tu-9=701). The obtained temperature for the leucosomes falls in the partial melting domain.

The equation of Watson and Harrison (2005):
 $LnD_{Zr} = [(1290 / T (K)) - 0.85(M-1) - 3.80$
 $M = [(Na+K+2Ca)/(Al,Si)]$



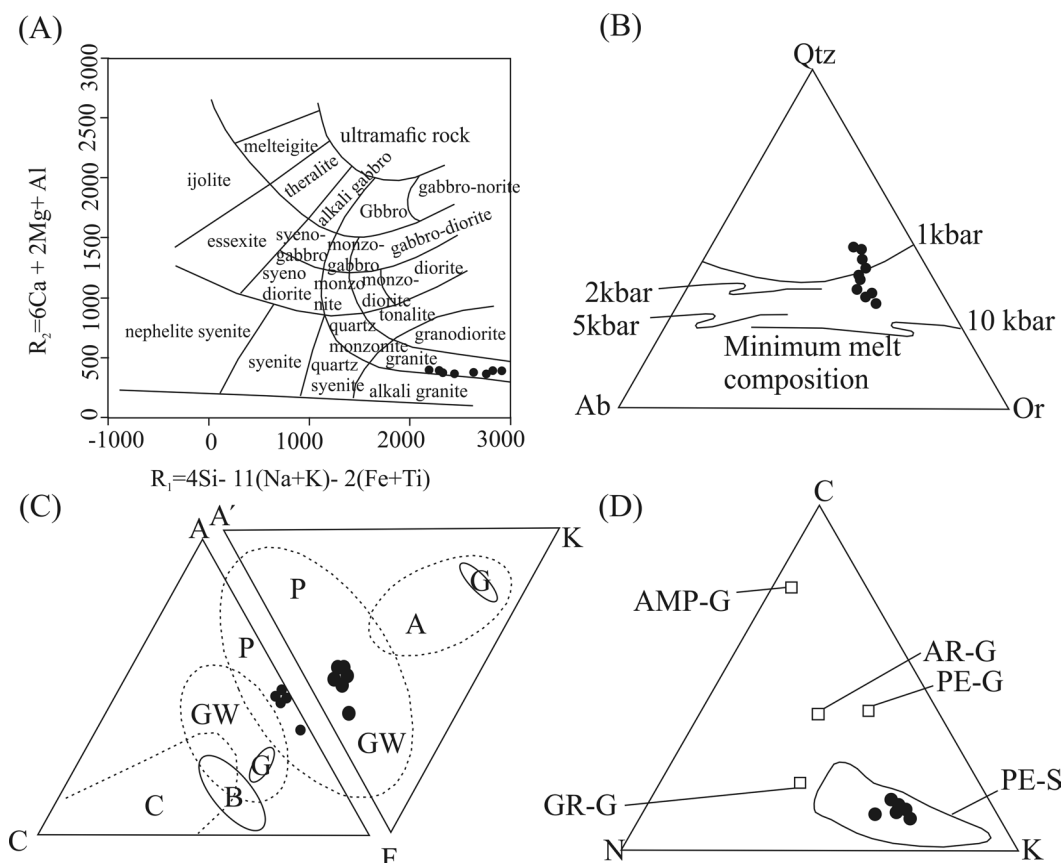


Figure 8. Chemical composition of mesosomes and leucosomes. A, B): leucosome composition, A: diagram is the R1-R2 classification diagram of De La Roche et al. (1980), B: triangular diagram is a Qtz-Ab-Or triangular plot with normative leucosome compositions and minimum melt compositions from Inger and Harris (1993). C, D): two triangular diagrams showing the chemical range observed on mesosomes from the Tuyserkan migmatites (A'FK, ACF and CNK triangles). For reference, plots also show average chemical compositions of rock types in central east China (AMP-G, amphibolite; AR-G, arenaceous; PE-G, pelite; GR-G, granulite; Gao et al., 1998) and range of pelite compositions (PE-S) from Shaw (1956). A: Andesite, B: Basalt, C: Carbonate rocks, G: Granitoid, GW: Gary Wake, P: Pelitic rocks from Winkler (1976).

Identifying a suitable source rock for partial melting

One important factor to identify partial melting with the help of trace elements in migmatites is identifying a suitable source rock. Leucosome migmatites in comparison with metapelites show higher amounts of Na_2O and K_2O and approximately P_2O_5 whereas mesosome migmatites have higher Al_2O_3 , Fe_2O_3 , MgO , MnO , TiO_2 and CaO (Tables 3, 4). This evidence along with field and petrographic observations show that the reason for such differences is the migration of felsic melts from metapelites that have undergone partial melting. The restitic nature of garnet, cordierite, biotite and calcic plagioclase minerals in the mesosome portion has resulted in the increases in the aforementioned oxides in mesosomes. The geochemical binary and spider diagrams (Figure 9) illustrate that the amount of Sr and Ba in migmatites (leucosome and mesosome) are more than metapelites

and in the leucosome portion of migmatites more than the mesosome portion that is representative of the fact that these elements have behaved incompatibly during the partial melting of metapelites and have entered the leucosome portion of migmatites. Considering the similar host mineral for Eu and Sr (plagioclase) and similar Sr/Y ratios, it is clear that like Sr, Eu has an incompatible nature and during partial melting enters leucosomes (melts). Y and Yb, however, are more enriched in mesosomes than in metapelites and leucosomes that show the compatible nature and subsequent accumulation of these elements in the restite (mesosome). The high Y and low Sr/Y ratio in mesosomes represent that during partial melting garnet has remained in the restite portion. As garnet hosts HREEs, this interpretation is accompanied by the fact that the mean HREEs and MREEs in the mesosome portion of migmatites are higher than metapelites. Among

Table 4. Major and trace element contents from leucosomes migmatites of Tuyserkan (Lu: leucosome).

Sample	Tu-11	Tu-12	Tu-13	Tu-14	Tu-15	Tu-10	Tu-17	Tu-16	Tu-8	Tu-9	Average
(%wt)	Lu	Lu	Lu								
SiO ₂	73.30	70.68	70.85	71.58	77.99	77.22	77.04	75.73	72.44	72.08	73.89
TiO ₂	0.02	0.18	0.12	0.20	0.10	0.16	0.08	0.16	0.11	0.07	0.12
Al ₂ O ₃	14.12	15.00	14.58	13.49	14.56	14.04	11.13	11.57	13.81	14.35	13.67
Fe ₂ O ₃	1.38	2.23	1.76	3.43	1.81	2.60	1.87	2.30	2.41	1.57	2.14
Cr ₂ O ₃	0.02	0.03	0.03	0.05	0.03	0.04	0.04	0.05	0.04	0.03	0.04
MnO	0.02	0.05	0.03	0.07	0.04	0.05	0.02	0.04	0.05	0.03	0.04
MgO	0.15	0.55	0.39	0.82	0.35	0.61	0.22	0.42	0.49	0.27	0.43
CaO	0.59	0.53	0.74	0.79	0.56	0.77	0.74	0.71	0.69	0.67	0.68
Na ₂ O	2.34	1.96	1.98	1.58	2.15	1.78	1.73	1.54	1.96	2.16	1.92
K ₂ O	6.87	7.29	7.77	5.88	7.08	6.83	5.73	5.94	6.38	7.32	6.71
P ₂ O ₅	0.17	0.18	0.19	0.19	0.18	0.19	0.14	0.14	0.18	0.18	0.17
Sum	98.98	98.68	98.44	98.08	104.9	104.3	98.74	98.60	98.56	98.73	99.80
(ppm)											
Cr	180	260	240	280	220	260	325	365	230	210	257
V	9	34	28	39	21.5	33.5	22.5	35	24	18.5	26.50
Cs	4.44	3.51	3.07	4.85	3.98	3.96	3.31	2.84	465.00	3.76	49.87
Rb	201	197.5	205	174.0	199.0	190.0	167.3	165.5	187.5	203.0	189.0
Sr	130.0	197.5	216	183.5	164.0	200.0	133.5	167.3	156.8	173.0	172.2
Ba	262	663	1170	1110	463	1140	587	878	686	716	768
Th	0.87	2.62	1.77	4.43	1.75	3.10	1.76	2.63	2.65	1.32	2.29
U	0.55	1.14	0.80	1.23	0.85	1.02	0.66	0.96	0.89	0.68	0.88
Ta	0.2	0.3	0.3	0.4	0.3	0.4	0.2	0.3	0.3	0.3	0.3
Nb	1.1	3.6	2.6	4.2	2.4	3.4	1.9	3.2	2.7	1.9	2.7
La	3.5	8.4	6.3	12.2	6.0	9.3	5.8	8.3	7.9	4.9	7.3
Ce	6.2	17.0	12.6	25.0	11.6	18.8	11.2	16.6	15.6	9.4	14.4
Pr	0.59	1.79	1.39	2.72	1.19	2.06	1.19	1.79	1.66	0.99	1.54
Nd	2.2	7.0	5.2	10.4	4.6	7.8	4.5	6.9	6.3	3.7	5.9
Sm	0.54	1.36	1.20	2.04	0.95	1.62	0.94	1.35	1.29	0.87	1.22
Eu	1.04	1.71	1.80	1.31	1.38	1.56	1.05	1.38	1.18	1.42	1.38
Gd	0.70	1.49	1.28	2.27	1.10	1.78	1.06	1.46	1.49	0.99	1.36
Tb	0.14	0.23	0.22	0.34	0.19	0.28	0.18	0.23	0.24	0.18	0.22
Dy	0.97	1.53	1.39	2.06	1.25	1.73	1.25	1.53	1.52	1.18	1.44
Ho	0.21	0.35	0.30	0.42	0.28	0.36	0.28	0.35	0.32	0.26	0.31
Er	0.66	0.98	0.93	1.18	0.82	1.06	0.92	1.08	0.92	0.80	0.94
Tm	0.11	0.15	0.13	0.17	0.13	0.15	0.14	0.16	0.14	0.12	0.14
Yb	0.70	0.97	0.85	0.99	0.84	0.92	0.88	1.01	0.85	0.78	0.88
Lu	0.10	0.14	0.12	0.14	0.12	0.13	0.13	0.15	0.12	0.11	0.13
Y	6.4	9.8	9.0	12.0	8.1	10.5	8.3	10.0	9.2	7.7	9.1
Hf	0.3	1.1	0.7	1.0	0.7	0.9	0.5	0.9	0.7	0.5	0.7
Zr	9	39	25	38	24	31.5	18.5	33.5	23.5	17	25.9
Ga	11.7	11.8	11.0	11.4	11.8	11.2	9.2	9.3	11.6	11.4	11.0
Sn	5	3	4	4	4	4	4	3	4.5	4.5	4
W	10	14	13	21	12	17	18	20	15.5	11.5	15.20
Nb/Ta	5.5	12	8.67	10.5	8	8.5	9.5	10.67	9	6.33	8.87
Zr/Hf	30	35.45	35.71	38	34.29	35	37	37.22	33.57	24.29	34.05
Rb/Sr	1.55	1	0.95	0.4	1.21	0.95	1.25	0.99	1.2	1.17	1.07
Sr/Ba	0.5	0.3	0.18	0.17	0.35	0.18	0.23	0.19	0.23	0.24	0.26
(La/Yb) _N	3.4	5.89	5.03	8.37	4.85	6.87	4.47	5.59	6.31	4.27	5.63
Eu*/Eu	0.2	0.47	0.41	0.7	0.34	0.56	0.33	0.46	0.46	0.3	0.42

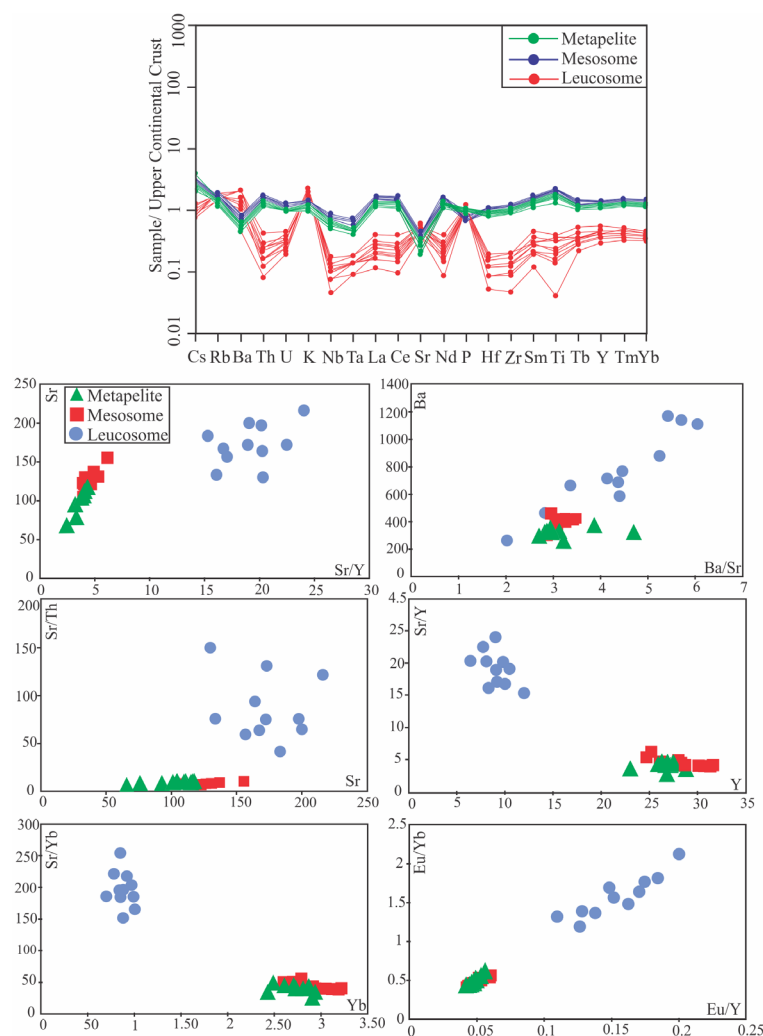


Figure 9. The geochemical binary and spider diagrams for metapelites and mesosome and leucosome migmatites normalized to the upper continental crust (normalizing values are from Taylor and McLennan, 1985).

lithophile elements, Sr and Ba are incompatible during partial melting and are able to enter the leucosome portion (showing positive anomaly). Leucosomes in relation to mesosomes and metapelites have lower REEs. It shows that these elements are stable during partial melting and remain in the mesosome portion. The spider diagram patterns of the mesosomes, leucosomes and metapelites show that the migmatites are produced by the partial melting of metapelites.

Pseudosections modeling for source rock of migmatites

Pressure and temperature at Tuyserkan area were estimated using whole rock composition and the observed mineral assemblages drawing pseudosections. In order to constrain the partial melting process and mineral assemblage development, the phase equilibrium modeling was carried out using thermocalc software

(Powell and Holland, 1988; v3.33) and internal data (Holland and Powell, 1998 tcds55.txt). All calculations were performed in the MnNCKFMASHT (MnO-Na₂O-CaO-K₂O-FeO-MgO-Al₂O₃-SiO₂-H₂O-TiO₂) with the following activity models: K-feldspar and plagioclase (Holland and Powell, 2003); silicate melt (White et al., 2007); muscovite (Coggon and Holland, 2002); biotite, garnet and ilmenite (White et al., 2005); orthopyroxene (White et al., 2002), cordierite (Holland and Powell, 1998; Mahar et al., 1997). Figure 10 shows the pressure and temperature pseudosection for the metapelitic samples (average metapelitic) under high temperature subsolidus to suprasolidus conditions. Considering the related pseudosection and based on the suprasolidus mineral assemblage and petrographic observations at the onset of melting more than 3.8 kbar pressures are needed. Higher than solidus the first main reaction that is related

to muscovite breakdown occurs that produces more than 5% melt. At this stage, the mineral assemblage consists of bi-sill-kfs-liq that is consistent with the observed minerals in the sillimanite zone. As the temperature rises the cordierite-K-feldspar zone appears during a process of cordierite substitution with biotite and sillimanite that the mineral assemblage features bi-cd-kfs-sill-liq. At the peak of cordierite-K-feldspar zone, sillimanite is consumed and the dominant assemblage in migmatites is peritectic cordierite and K-feldspar (And-bi-cd-ksp-liq). The stability field of this assemblage is limited by garnet line at pressures lower than 4.4 kbar. The silicate melt for metapelite at the conditions of cordierite-K-feldspar zone (pressure 4.3kbar and temperature 700 °C) is predicted to be more than 10 mol% (Figure 10). As the temperature

increases (more than 700 °C) spinel-cordierite zone appears that is illustrated by the stability field of the And-bi-spl-cd-kfs-liq. As it is demonstrated in the figure 10 the stability fields of this assemblage are limited by garnet line at pressures lower than 3.7 kbar and the generated melt is predicted to be more than 20% at peak metamorphic conditions (spinel-cordierite zone, p=3.8 kbar and temperature more than 700 °C). The estimated temperature using multi-equilibrium curves and the average P-T with the help of thermocalc software for peak metamorphic conditions (spinel-cordierite zone) (T=700 and 729 °C respectively) lies in the field of the predicted assemblage (And-bi-spl-and-cd-kfs-liq). Figure 11 shows the pressure and temperature pseudosection for the migmatite sample Tu-10 in the spinel-cordierite zone (peak metamorphism).

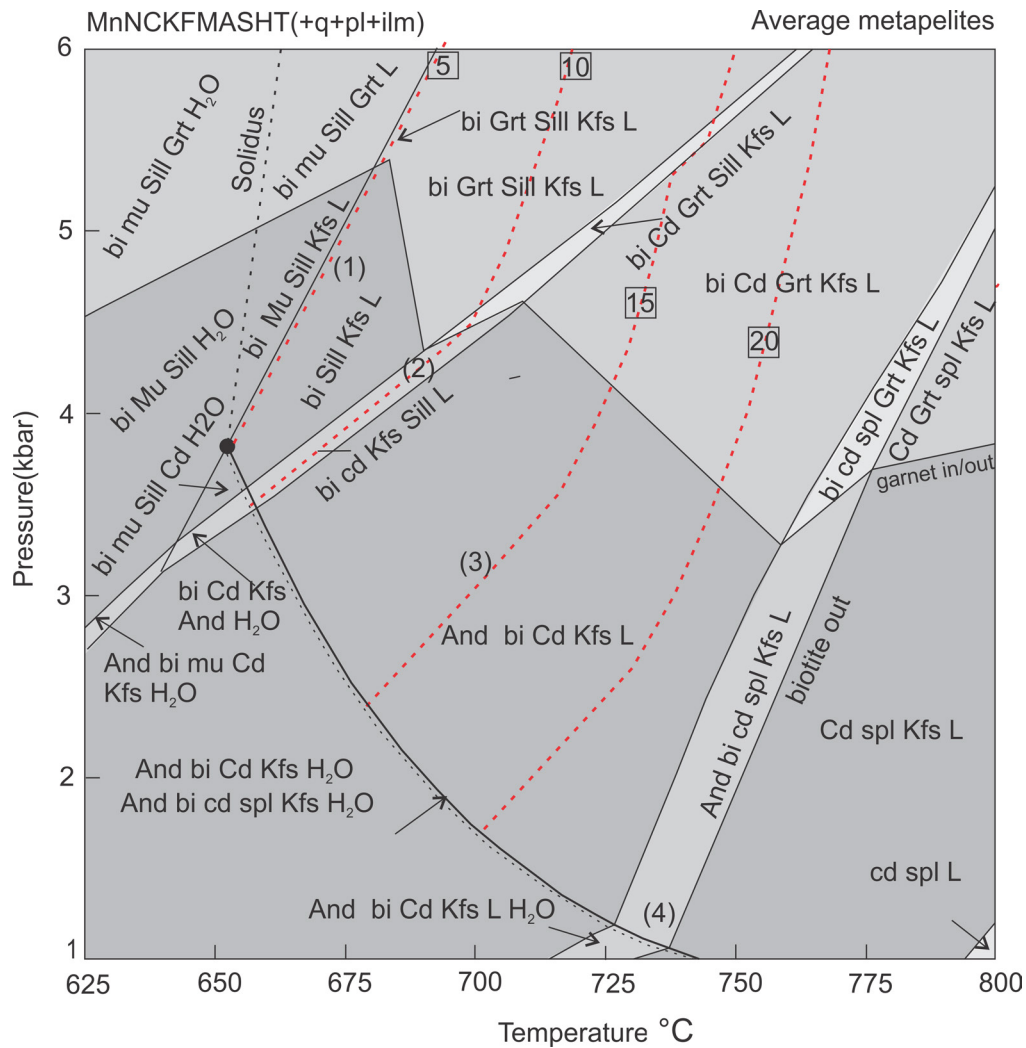


Figure 10. Pressure and temperature pseudosection in the system MnNCKFMASHT for metapelites along with isopleths. The amounts of partial melting are written in rectangles. The numbers in the fields are consistent with the mineral assemblages observed in petrographic studies.

The observed assemblages in the sample Tu-10 agreements with the stability field of the bi-spl-and-cd-ksp-liq assemblage that lies to the right in the metapelite diagram from 1 to 3.7 kbar and 725 °C. As a whole the registered path by the rock shows a low-pressure path along which the peak metamorphic condition is about 3.7 kbar and 725 °C. The peak metamorphic assemblages are preserved in the cordierite-spinel zone in the mesosomes is consistent with the extraction of a large amount of melt. Otherwise, the metamorphic assemblages during melt crystallization would be retrograde (Guiraud, Powell and Rebay, 2001; White and Powell, 2002). Among the melt extraction evidences, the abundant peritectic minerals and anhydrous minerals, like cordierite and K-feldspar along with low amounts of leucosome, could be mentioned. Considering the pseudosection (Figure 11), the amount of the extracted melt is more than 25 %mole that has been

modeled at peak metamorphic conditions at 3.7 kbar and 725 °C in metapelites (Figure 12). In this modeling, it is demonstrated that the composition of the restite with the extraction of 25% of melt from metapelites by biotite dehydration reactions (fluid-absent reactions) lies in the field of And-bi-spl- cd-kfsp. The result of this model is similar to the calculated pseudosection for migmatites (mesosome) in spinel-cordierite zone (Figure 10) that is representative of migmatites being generated from the partial melting of metapelites.

Leucosome and mesosome geochemistry

Figure 13 reports the REE diagram for the mesosome and leucosome rocks normalized to chondrite (normalizing values are from Boyton, 1984) and average REE content of the upper continental crust from Rudnick and Gao (2003). The REE patterns in leucosomes show REE enrichment

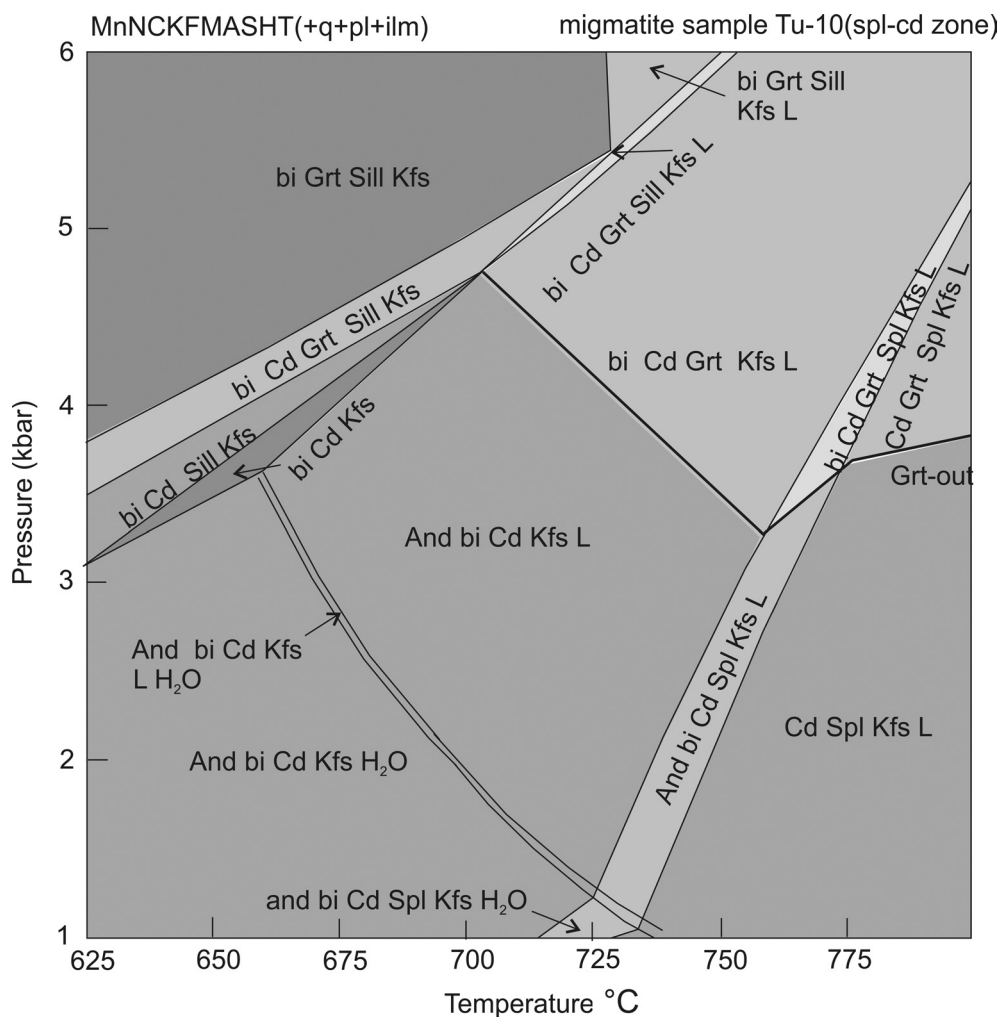


Figure 11. Pressure and temperature pseudosection that shows the phase relations for the TU-10 sample from spinel-cordierite zone. The related field (bolded) is the observed mineral assemblage in this sample.

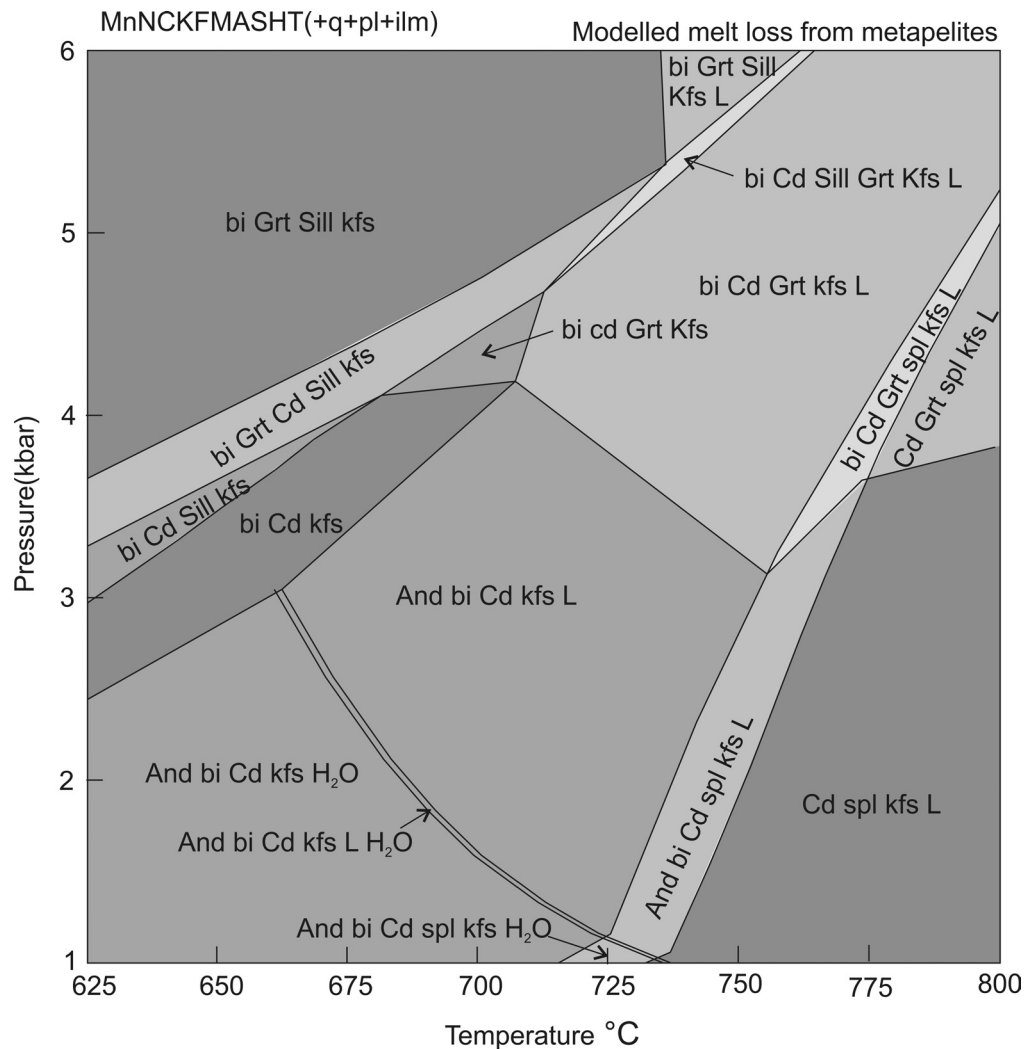


Figure 12. Pressure and temperature pseudosection for the migmatite sample of TU-12 from which 20 % mole melt has been extracted at peak metamorphic conditions (725 °C and almost 4 kbar). In this modeling the restite from metapelites lies in the stability field of bi-spl-and-cd-ksp-liq that is similar to the results of the modeling of the calculated pseudosection for migmatites (mesosome) from spinel-cordierite zone (Figure 11).

and LREEs are more enriched than HREEs and Eu shows a positive anomaly (Figure 13). The low concentration of HREEs in relation to LREEs is controlled by low partial melting rate and garnet remaining in the source region as mesosome. The Eu anomaly is controlled largely by feldspars because Eu is compatible in plagioclase and feldspar (Rollinson, 1993). The positive anomaly is representative of feldspar differentiation (Xu et al., 2007). This pattern is consistent with the leucosome composition that has alkali-feldspar granite composition. Leucosomes have REE contents lower than the average REE content of the upper continental crust. Moreover, the REE patterns of mesosome samples show mostly similar trends. Mesosomes have flat HREE and MREE patterns and negative Eu anomalies. They are enriched in LREEs

and have similar pattern and REE content to the average REE content of the upper continental crust (Rudnick and Gao, 2003). The HREE pattern is flat that shows the lower amount of these elements in the source rock.

DISCUSSION

P-T conditions of the migmatites (Geothermobarometry) and its implications

Figure 14 shows a summary of pressure and temperature estimates of migmatites from the Tuyserkan area calculated using the multiple equilibria routine of Thermocalc (v. 3.3, Powell and Holland, 1988) and the internally consistent thermodynamic database of Holland and Powell (1998; tcds55). The estimated temperature for Tuyserkan migmatites is about 700 °C. The pressure of metamorphism

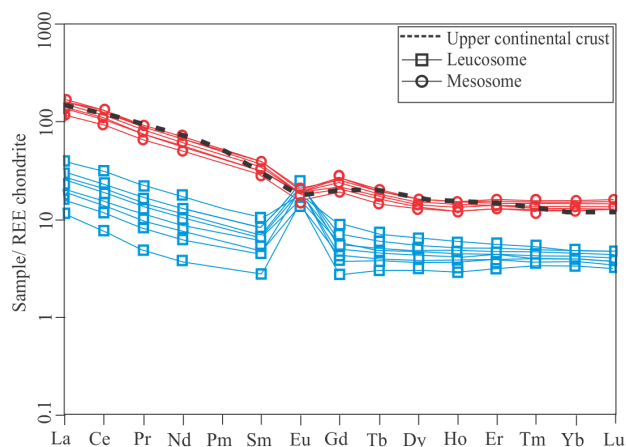


Figure 13. Rare-earth element (REE) diagram for mesosome and leucosome rocks normalized to chondrite (normalizing values are from Boyton (1984); average REE content of the upper continental crust from Rudnick and Gao (2003).

was estimated as 3.8 kbar. The activities of all minerals needed in these calculations are determined through AX software (Holland and Powell, 1988). Based on these data the depth of metamorphism in Tuyserkan area was about 13 km and geothermal gradient was computed as 54 °C /km. These data are consistent with contact metamorphism and Buchan metamorphic zones and correlate with low-pressure/high-temperature metamorphism. Table 2 represents details about activities and the reactions considered in the calculations in the KFMASH system by THERMOCALC. Also, the estimated temperature and pressure for Tuyserkan migmatites using the average P-T routine of Thermocalc (v. 3.3, Powell and Holland, 1998) is 729 °C and 4.2 kbar,

respectively. Thermometry, using several methods, was carried out over intrusive bodies (gabbros) by Sepahi et al. (2012) and the temperature for gabbros and olivine gabbros was estimated as 950 °C and 1300 °C, respectively. Moreover, considering the contact metamorphic reactions the maximum temperature at the contact of porphyritic granites (Alvand intrusive) was estimated between 530 °C and 550 °C (Sepahi et al., 2001). Such a temperature is not enough for migmatization. This is representative of the fact that anatexis and partial melting did not occur because of granitic intrusions but migmatites were formed during contact metamorphism due to the injection of mafic intrusions that are synchronous with migmatites.

Geochemical implications for migmatite

The geochemistry of leucosomes and adjacent granites in Tuyserkan area.

The granites in the area include porphyroid granites and porphyroid leucocratic granites. Considering the large volume of porphyroid granites in relation to migmatites it is not possible for migmatites to feed granites that is to say contact metamorphism is not capable of generating a large and voluminous batholith as is observed in this area, but considering the limited volume of leucogranites and the similarity between leucosomes and leucogranites it is possible for the migmatites to feed granites. In order to investigate the source and potential relationships between leucosomes and adjacent granites (leucocratic granites) the comparison between the chemical compositions of these rocks was performed. The chemical composition of leucocratic granites and leucosomes are illustrated in Tables 4 and 5. Leucocratic granites are distributed in the Alvand granitoids and metamorphic rocks in the form of

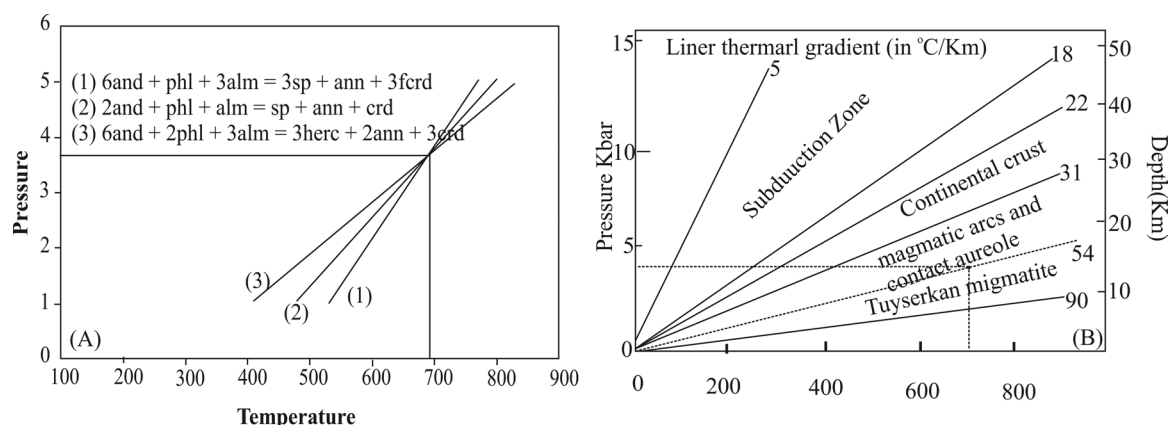


Figure 14. A: P-T grid for the metapelites in the KFMASH system. Representative results of multiple equilibria calculated by THERMOCALC [reactions (1)-(3)] are presented. A pressure of 3.8 kbar and temperature of ~700 °C can be deduced for peak metamorphism. B: The linear relationship between temperature and depth is indicative of geothermal gradient (Holdaway and Mukhopdhyay, 1993). The geothermal gradient of the Tuyserkan migmatites is depicted by a dotted line that lies in the contact metamorphic field.

centimeter- to meter-thick veins and elongated bodies (Aliani et al., 2011). In this comparison, leucocratic granites next to the migmatites and centimeter-thick leucosomes are considered. The leucocratic granites that lie next to the migmatites reach up to centimeter- to meter-scale in thickness. These granites are bright in color

and mainly composed of quartz, K-feldspar, muscovite, biotite and garnet.

Major elements: the constituent components of feldspars (K_2O and Al_2O_3) are high in leucocratic granites. The $Na/Na+Ca$ ratio is higher in leucocratic granites than in leucosomes. The SiO_2 content and the constituents of

Table 5. Major and trace element contents from granites of Tuyserkan (G: granite).

Sample	Tu-17	Tu-18	Tu-19	Tu-20	Tu-21	Tu-10	Tu-12	Tu-14	Tu-15	Tu-11	Average
(%wt)	G	G	G	G	G	G	G	G	G	G	G
SiO_2	72.72	72.84	71.98	72.44	72.50	72.47	72.21	72.24	72.67	72.61	72.47
TiO_2	0.03	0.04	0.03	0.05	0.03	0.04	0.04	0.03	0.04	0.03	0.04
Al_2O_3	14.29	14.16	14.28	14.26	14.24	14.25	14.27	14.26	14.20	14.27	14.25
Fe_2O_3	1.70	1.59	1.98	1.47	1.64	1.56	1.73	1.81	1.20	1.67	1.64
Cr_2O_3	0.03	0.04	0.04	0.03	0.03	0.03	0.04	0.04	0.04	0.03	0.04
MnO	0.11	0.06	0.11	0.08	0.09	0.09	0.10	0.10	0.08	0.10	0.09
MgO	0.14	0.13	0.20	0.13	0.13	0.13	0.17	0.17	0.13	0.14	0.15
CaO	0.46	0.87	0.43	0.44	0.50	0.47	0.44	0.47	0.69	0.48	0.53
Na_2O	2.32	2.61	2.37	2.31	2.39	2.35	2.34	2.38	2.50	2.36	2.39
K_2O	7.71	6.49	7.57	7.89	7.61	7.75	7.73	7.59	7.05	7.66	7.51
P_2O_5	0.22	0.14	0.22	0.23	0.22	0.23	0.23	0.22	0.18	0.22	0.21
Sum	99.73	98.97	99.21	99.33	99.38	99.37	99.30	99.31	98.78	99.57	99.29
(ppm)											
Cr	240	280	300	210	240	225	255	270	260	240	252
V	8	11	10	8	9	8.5	9	9.5	10	8.5	9.15
Cs	3.67	3.42	2.56	3.87	3.40	3.64	3.22	2.98	3.41	3.54	3.37
Rb	217	175.5	212	223	208	216	218	210	192	213	208
Sr	106.0	105.0	100.5	109.5	103.5	106.5	105.0	102.0	104.3	104.8	104.7
Ba	161.5	178.0	188.0	168.5	141.5	155.0	178.0	165.0	160.0	152.0	164.8
Th	0.97	1.28	0.53	0.89	0.71	0.80	0.71	0.62	1.00	0.84	0.84
U	0.84	0.50	0.64	1.00	1.55	1.28	0.82	1.10	1.03	1.20	1.00
Ta	0.1	0.1	0.1	0.3	0.2	0.3	0.2	0.2	0.2	0.2	0.2
Nb	1.1	0.9	0.9	2.2	1.3	1.8	1.6	1.1	1.1	1.2	1.3
La	3.6	4.7	3.1	3.8	3.3	3.6	3.5	3.2	4.0	3.5	3.6
Ce	6.8	8.7	5.6	7.0	5.8	6.4	6.3	5.7	7.3	6.3	6.6
Pr	0.73	0.87	0.61	0.78	0.62	0.70	0.70	0.62	0.75	0.68	0.71
Nd	2.8	3.0	2.2	3.0	2.4	2.7	2.6	2.3	2.7	2.6	2.6
Sm	0.77	0.65	0.58	0.82	0.63	0.73	0.70	0.61	0.64	0.70	0.68
Eu	0.78	0.79	0.76	0.82	0.78	0.80	0.79	0.77	0.79	0.78	0.79
Gd	1.15	0.60	1.01	1.26	0.95	1.11	1.14	0.98	0.78	1.05	1.00
Tb	0.26	0.11	0.25	0.25	0.23	0.24	0.25	0.24	0.17	0.25	0.23
Dy	2.52	1.04	2.31	2.20	2.00	2.10	2.26	2.16	1.52	2.26	2.04
Ho	0.67	0.28	0.59	0.54	0.52	0.53	0.57	0.56	0.40	0.60	0.53
Er	2.61	1.17	2.30	2.14	2.01	2.08	2.22	2.16	1.59	2.31	2.06
Tm	0.49	0.22	0.47	0.40	0.42	0.41	0.44	0.45	0.32	0.46	0.41
Yb	4.15	1.90	3.71	3.22	3.24	3.23	3.47	3.48	2.57	3.70	3.27
Lu	0.66	0.34	0.58	0.53	0.53	0.53	0.56	0.56	0.44	0.60	0.53
Y	19.4	8.0	18.1	16.6	15.2	15.9	17.4	16.7	11.6	17.3	15.6
Hf	1.3	0.5	1.1	1.6	1.5	1.6	1.4	1.3	1.0	1.4	1.3
Zr	29	15	25	37	35	36	31	30	25	32	29.50
Sn	4	5	3	4	4	4	3.5	3.5	4.5	4	3.95
W	13	16	16	12	14	13	14	15	15	13.5	14.15
Eu*/Eu	0.31	0.21	0.25	0.33	0.25	0.3	0.29	0.25	0.23	0.23	0.27
(La/Yb) _N	0.59	1.64	0.57	0.8	0.69	0.76	0.7	0.62	1.06	0.64	0.75

mafic minerals (MgO, FeO and TiO₂) in leucosomes are more than leucocratic granites and show high contents of the Mg/Mg+Fe ratio (Tables 4, 5). These amounts show that the adjacent granites and leucosomes do not share a similar source. In other words, the adjacent granites and migmatites are not co-genetic.

Trace elements: Leucosomes and leucocratic granites show substantial variations in trace and major elements. Granites are higher in some HFSE elements (Y, Yb) and leucosomes are higher in the elements that preferably enter plagioclase (Eu) (Tables 4, 5, Figure 15).

HREE elements: Chondrite-normalized REE patterns for leucocratic granites are illustrated in Figure 15. These patterns show enrichments in HREEs and LREEs and are identified with a positive Eu-anomaly. The presence of garnet in granites has resulted in the enrichment of HREE elements. The REE pattern for leucosomes is different from this pattern for leucocratic granites. The most important feature of REE patterns is the difference in HFSE amounts between granites and leucosomes. The lower HREE content in leucosomes, in comparison with leucocratic granites, is because of the lack of garnet in leucosome portion of migmatites. The obvious difference in the amount of rare earth elements and the HREE patterns between leucocratic granites and leucosome portion of migmatites show that there is not a genetic relationship between migmatites and the adjacent granites. Shahbazi et al. (2010) estimated the age of Alvand plutonic rocks for leucocratic granites at 154.4±1.3 and 153±2.7 Ma. Sepahi et al. (2018) age dated the Tuyserkan migmatites at 160-180 Ma and an average of 170 Ma that is almost the same as the Alvand pluton. The REE pattern of leucosomes and the adjacent granites as well as the geochronological

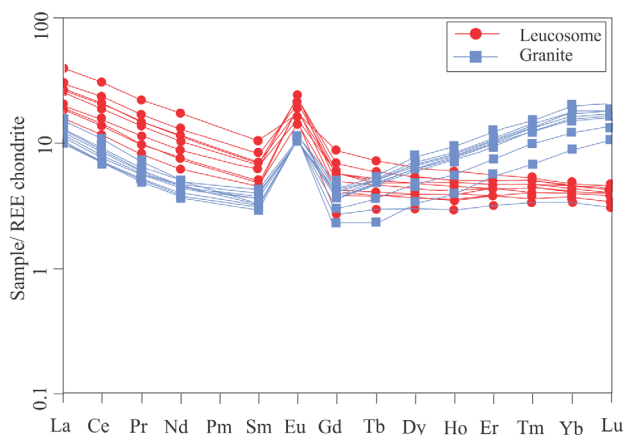


Figure 15. Chondrite-normalized REE diagram of the granites observed adjacent to the migmatites and leucosome layers in Tuyserkan area. For normalization, the values of chondrites of Boynton (1984) have been used.

studies show that leucosomes and leucocratic granites are not co-genetic and leucocratic granites are younger and have been injected after migmatization and leucocratic granites of adjacent are not the result of partial melting of migmatites.

CONCLUSIONS

Based on the field studies, petrography, mineralogy, thermobarometry and geochemical data the following results are obtained:

The intrusion of Alvand batholith, that belong to Jurassic, into the metamorphosed pelitic rocks have resulted in the formation of pelitic hornfels and partial melting migmatites in the Alvand aureoles. Partial melting was not extensive and it was at microscopic to macroscopic scale. Leucosomes are dominantly composed of quartz and feldspar and have igneous texture. The textural difference between leucosome and melanosome portions (leucosomes have igneous texture whereas melanosome has hornfels texture), the mineralogical composition of leucosomes that is composed by quartz and feldspar, the distribution of the melt in the rocks and the estimated pressure and temperature all confirm the anatexis origin for the leucosomes. Fluid-present melting reactions may have consumed the whole free fluid in the aureole and hence, the partial melting has proceeded through fluid-absent reactions. With a high possibility, high-grade minerals like spinel in the aureole are formed through fluid-absent reactions (biotite dehydration reactions). The presence of spinel in these rocks is representative of the passing from hornblende hornfels facies to pyroxene hornfels facies that is related to partial melting through the lack of free fluid processes. The peak metamorphic conditions in Tuyserkan migmatites are estimated at T=700 °C and P=3.8 that reflect high-temperature/low-pressure metamorphism. The REE pattern of leucosomes and the adjacent granites as well as the geochronological studies show that leucosomes and leucocratic granites are not co-genetic and leucocratic granites are younger and have been injected after migmatization and leucocratic granites of adjacent are not the result of partial melting of migmatites. In addition to geothermobarometric calculations of migmatites and intrusive bodies as well as the dating that are performed on Alvand plutonic intrusion and migmatites confirm that anatexis and partial melting are not the result of granitic intrusions but the result of the temperature released from old mafic bodies. Thus, migmatites are formed by the injection of mafic intrusions that are synchronous with them.

ACKNOWLEDGEMENTS

These research result are part of the Ph.D. thesis of Masoumeh Zare-Shooli supported by the grant of Professor Zhai Mingguo at Chinese Academy of Sciences. We are grateful for the

financial support of Professor Zhai Mingguo and his grant at Chinese Academy of Sciences. We acknowledge support from Priority Strategic Program (XDB18030205) and Chinese Academy of Sciences. We thank from the Southwest Petroleum University Laboratory, division of key Laboratory Carbonate, Reservoirs, CNPC, Chengdu, 610500, China. Also we thank from the financial support of Lorestan University and Mr. Rasoul Esmaeili from university of Chinese Academy of Sciences for his help in doing the electron microprobe analysis. The authors thank the editor and reviewers for their valuable comments and suggestions that improved the manuscript significantly.

REFERENCES

- Alavi M., 1994. Tectonics of Zagros orogenic belt of Iran: new data and interpretation. *Tectonophysics* 229, 211-238.
- Aliani F., Sabouri Z., Maanijou M., Sepahi A.A., 2011. Lithology and Geochemistry of hololeucocrate granitoids of Alvand granitoid mass (Hamadan). *Iranian Journal of Crystallography and Mineralogy* 19, 133-144 (in Persian).
- Antipin V.S., Kushch L.V., Sheptyakova N.V., Vladimirov A.G., 2018. Geochemical evolution of the early Paleozoic collisional magmatism from autochthonous migmatites and granitoids to multiphase granite intrusions (Sharanur and Aya complexes, Baikal Region). *Russian Geology and Geophysics* 59, 1616-1625.
- Baharifar A., Moinevaziri H., Bellon H., Pique A., 2004. The crystalline complexes of Hamadan (Sanandaj-Sirjan zone, western Iran): Metasedimentary Mesozoic sequences affected by Late Cretaceous tectono-metamorphic and plutonic events, ^{40}K - ^{40}Ar dating. *Comptes Rendus Geoscience* 366, 1443-1452.
- Baharifar A.A., 2004. Petrology of metamorphic rocks in the Hamedan area. Ph.D. thesis, Tarbiat Moallem University, Tehran, Iran (in Persian).
- Berberian M. and King G.C., 1981. Towards a paleogeography and tectonic evolution of Iran. *Canadian Journal of Earth Sciences* 18, 210-265.
- Boynton W.V., 1984. Cosmochemistry of the rare earth elements; meteorite studies. In: Henderson, P. (Ed.), *Rare earth element geochemistry. Developments in Geochemistry* 2, 63-114.
- Chappell B.W. and White A.J.R., 1974. Two contrasting granite types. *Pacific Geology* 8, 173-174.
- Chen Y.X., Gao P., Zheng Y.F., 2015. The anatectic effect on the zircon Hf isotope composition of migmatites and associated granites. *Lithos* 238, 174-184.
- Chiu H.Y., Chung S.L., Zarrinkoub M.H., Mohammadi S.S., Khatib M.M., Iizuka Y., 2013. Zircon U-Pb age constraints from Iran on the magmatic evolution related to Neotethyan subduction and Zagros orogeny. *Lithos* 162, 70-87.
- Clemens J.D., 2003. S-type granitic magmas- petrogenetic issues, models and evidence. *Earth-Science Reviews* 61, 1-18.
- Coggon R. and Holland T.J.B., 2002. Mixing properties of phengitic micas and revised garnet-phengite thermobarometers. *Journal of Metamorphic Geology* 20, 683-696.
- Corona-Chavez P., Poli S., Bigioggero B., 2006. Syn-deformational migmatites and magmatic-arc metamorphism in the Xolapa Complex, southern Mexico. *Journal of metamorphic Geology* 24, 169-191.
- De La Roche H., Leterrier J., Grandclaude P., Marchal M., 1980. A classification of volcanic and plutonic rocks using R1-R2 diagram and major-element analyses-its relationships with current nomenclature. *Chemical Geology* 29, 183-210.
- Droop G.T.R. and Moazzen M., 2007. Contact metamorphism and partial melting of Dalradian pelites and semipelites in the southern sector of the Etive aureole. *Scottish Journal of Geology* 43, 155-179.
- Fyfe W.S., 1973. The granulite facies, partial melting and the Archaean crust. *Philosophical Transactions of the Royal Society of London, series A* 273, 457-461.
- Guiraud M., Powell R., Rebay G., 2001. H₂O in metamorphism and unexpected behavior in the preservation of metamorphic mineral assemblages. *Journal of Metamorphic Geology* 19, 445-454.
- Harris N., Ayres M., Massey, J., 1995. Geochemistry of granitic melts produced during the incongruent melting of muscovite-implications for the extraction of Himalayan leucogranite magmas. *Journal of Geophysical Research* 100, 15767-15777.
- Harris N.B.W. and Inger S., 1992. Trace element modelling of pelite-derived granites. *Contributions to Mineralogy and Petrology* 110, 46-56.
- Holdaway M.J. and Mukhopadhyay B., 1993. A re-evaluation of the stability relations of andalusite: thermochemical data and phase diagram for the aluminum silicates. *American Mineralogy* 78, 298-315.
- Holland T. and Powell R., 2003. Activity-compositions relations for phases in petrological calculations: An asymmetric multicomponent formulation. *Contributions to Mineralogy and Petrology* 145, 492-501.
- Holland T.J.B. and Powell R., 1998. An internally consistent thermodynamic data set for phases of petrological interest. *Journal of Metamorphic Geology* 16, 309-343.
- Inger S. and Harris N., 1993. Geochemical constraints on leucogranite magmatism in the Langtang Valley, Nepal Himalaya. *Journal of Petrology* 34, 345-368.
- Jafari S.R., 2007. Petrology of Migmatites and Plutonic Rocks of South Simin Area, Hamadan. M.Sc. thesis, Bu Ali Sina University, Hamedan, Iran (in Persian).
- Johannes W. and Gupta L.N., 1982. Origin and evolution of a migmatite. *Contributions to Mineralogy and Petrology* 79, 114-123.
- Kalsbeek F., Jepsen H.F., Jones A., 2001. Geochemistry and petrogenesis of S-type granite in East Greenland Caledonides. *Lithos* 57, 91-109.
- Kriegsman L.M., 2001. Partial melting, partial melt extraction and partial back reaction in anatectic migmatites. *Lithos* 56,

- 75-96.
- Lancaster J., Fu B., Page F.Z., Kita N.T., Bickford M.E., Hill B.M., McLelland J.M., Valley J.W., 2009. Genesis of metapelitic migmatites in the Adirondack Mountains. *Journal of Metamorphic Geology* 27, 41-54.
- Mahar E.M., Baker J.M., Powell R., Holland T.J.B., Howell N., 1997. The effect of Mn on mineral stability in metapelites. *Journal of Metamorphic Geology* 15, 223-238.
- Mahmoudi S., Corfu F., Masoudi F., Mehrabi B., Mohajjel M., 2011. U-Pb dating and emplacement history of granitoid plutons in the northern Sanandaj-Sirjan Zone, Iran. *Journal of Asian Earth Sciences* 41, 238-249.
- Marchildon N. and Brown M., 2002. Grain-scale melt distribution in two contact aureole rocks: implications for controls on melt localization and deformation. *Journal of Metamorphic Geology* 20, 381-396.
- Marchildon N. and Brown M., 2003. Spatial distribution of melt-bearing structures in anatectic rocks from Southern Brittany, France: implications for melt transfer at grain to orogen-scale. *Tectonophysics* 364, 215-235.
- Mohajjel M. and Fergusson C.L., 2000. Dextral transpression in Late Cretaceous continental collision, Sanandaj-Sirjan Zone, western Iran. *Journal of Structural Geology* 22, 1125-1139.
- Mohajjel M., Fergusson C.L., Sahandi M.R., 2003. Cretaceous-Tertiary convergence and continental collision, Sanandaj-Sirjan Zone, Western Iran. *Journal of Asian Earth Sciences* 21, 397-412.
- Patino-Douce A.E. and Harris N., 1998. Experimental constraint on Himalayan anatexis. *Journal of Petrology* 39, 689-710.
- Powell R. and Holland T.J.B., 1988. An internally consistent dataset with uncertainties and correlations: 3. Applications to geobarometry, worked examples and a computer program. *Journal of Metamorphic Geology* 6, 173-204.
- Rollinson H., 1993. Using geochemical data: evolution, presentation, interpretation, Longman Ltd., London, U.K.
- Rudnick R.L., 1995. Making continental crust. *Nature* 378, 571-578.
- Rudnick R.L. and Gao S., 2003. Composition of the continental crust. *Treatise on Geochemistry* 3, 1-64.
- Saki A., 2010a. Proto-Tethyan remnants in northwest Iran: Geochemistry of the gneisses and metapelitic rocks. *Gondwana Research* 17, 704-714.
- Saki A., 2010b. Mineralogy, geochemistry and geodynamic setting of the granitoids from NW Iran. *Geological Journal* 45, 1-16.
- Saki A., 2011. Formation of spinel-cordierite-plagioclase symplectites replacing andalusite in metapelitic migmatites of the Alvand aureole, Iran. *Geological Magazine* 148, 423-434.
- Saki A., Moazzen M., Baharifar A.A., 2012. Migmatite microstructures and partial melting of Hamadan metapelitic rocks, Alvand contact aureole, western Iran. *International Geology Review* 54, 1229-1240.
- Sawyer E.E., 2008. Working with migmatite, Mineralogical Association of Canada Short Course. Quebec City, Quebec 38, 1-168.
- Sawyer E.W. and Barnes S.J., 1988. Temporal and compositional differences between subsolidus and anatectic migmatite leucosomes from the Quetico metasedimentary belt, Canada. *Journal of Metamorphic Geology* 6, 437-450.
- Sawyer E.W. and Barnes S.J., 1988. Temporal and compositional differences between sub-solidus and anatectic migmatite leucosomes from the Quetico metasedimentary belt, Canada. *Journal of Metamorphic Geology* 6, 437-450.
- Sepahi A.A., Jafari, S.R., Mani-Kashani S., 2009. Low pressure migmatites from the Sanandaj-Sirjan Metamorphic Belt in the Hamedan region (Iran). *Geologica Carpathica* 60, 107-119.
- Sepahi A.A., 1999. Petrology of the Alvand plutonic complex with special reference on granitoids. Ph. D. Thesis, Tarbiat-Moallem University, Tehran, Iran (in Persian).
- Sepahi A.A., Borzoei K., Salami S., 2012. The study of minerals chemistry, thermobarometry and tectonic setting of plutonic rocks from Sarabi Tueyserkan area (Hamedan province). *Petrology* 3, 39-58 (in Persian with English abstract).
- Sepahi A.A., Borzoei K., Salami S., 2013. Mineral chemistry and thermobarometry of plutonic, metamorphic and anatectic rocks from the Tueyserkan area (Hamedan, Iran). *Geological Quarterly* 57, 515-526.
- Sepahi A.A. and Moein Vaziri H., 2001. New findings on metamorphic rocks and adjacent megametates of the Alvand plutonic complex. *Journal of Basic Sciences Isfahan University* 15, 37-52 (In Persian).
- Sepahi A.A., Shahbazi H., Siebel W., Ranin A., 2014. Geochronology of plutonic rocks from the Sanandaj-Sirjan zone, Iran and new zircon and titanite U-Th-Pb ages for granitoids from the Marivan pluton. *Geochronometria* 41, 207-215.
- Sepahi A.A., Whitey D.L., Baharifar A.A., 2004. Petrogenesis of Andalusite-Kyanite-Sillimanite veins and host rocks, Sanandaj-Sirjan metamorphic belt, Hamedan, Iran. *Journal of Metamorphic Geology* 22, 119-134.
- Sepahi A.A., Jafari S.R., Osanai Y., Shahbazi H., Moazzen M., 2018. Age, petrologic significance and provenance analysis of the Hamedan low-pressure migmatites; Sanandaj-Sirjan Zone, West Iran. *International Geology Review*.
- Shahabpour J., 2005. Tectonic evolution of the orogenic belt in the region located between Kerman and Neyriz. *Journal of Asian Earth Sciences* 24, 405-417.
- Shahbazi H., Siebe W., Pourmoafee M., Ghorbani M., Sepahi A.A., Shang C., Abedini M.V., 2010. Geochemistry and U-Pb zircon geochronology of the Alvand plutonic complex in Sanandaj-Sirjan Zone (Iran): New evidence for Jurassic magmatism. *Journal of Asian Earth Sciences* 39, 668-683.
- Shand S.J., 1943. Eruptive rocks: their genesis, composition, classification and their relation to ore-deposits, with a chapter on meteorites, Thomas Murby and Co., London.
- Shaw D.M., 1956. Geochemistry of pelitic rocks. Part iii: major

- elements and general geochemistry. *Bulletin of the Geological Society of America* 67, 919-934.
- Taylor S.R. and McLennan S.H., 1985. *The Continental Crust: Its Composition and Evolution*, Blackwell, Oxford.
- Toe W., Vanderhaeghe O., Andre-Mayer A.S., Feybesse J.L., Milesi J.P., 2013. From migmatites to granites in the Pan-African Damara orogenic belt, Namibia. *Journal of African Earth Sciences* 85, 62-74.
- Vielzeuf D. and Holloway J.R., 1988. Experimental determination of the fluid-absent melting relations in the pelitic system. *Contributions to Mineralogy and Petrology* 98, 257-276.
- Wang Y., Zhou Y., Cai Y., Liu H., Zhang Y., Fan W., 2016. Geochronological and geochemical constraints on the petrogenesis of the Ailaoshan granitic and migmatite rocks and its implications on Neoproterozoic subduction along the SW Yangtze Block. *Precambrian Research* 283, 106-124.
- Watson E.B. and Harrison T.M., 2005. Zircon thermometer reveals minimum melting conditions on earliest Earth. *Science* 308, 841-844.
- Weber C. and Barbey P., 1986. The role of water, mixing processes and metamorphic fabric in the genesis of the Baume migmatites (Ardèche, France). *Contributions to Mineralogy and Petrology* 92, 481-491.
- Whalen J., McNicoll J., Van Staal C.R., Frederick C.J.L., Longstaffe J., Jenner G., Van B., 2006. Spatial, temporal and geochemical characteristics of silurian collision-zone magmatism, Newfoundland Appalachians: An example of a rapidly evolving magmatic system related to slab break-off. *Lithos* 89, 377-404.
- White A.J.R. and Chappell B.W., 1977. Ultrametamorphism and granitoid genesis. *Tectonophysics* 43, 7-22.
- White R.W., Pomroy N.E., Powell R., 2005. An in situ metatexite-diatexite transition in upper amphibolite facies rocks from Broken Hill, Australia. *Journal of Metamorphic Geology* 23, 579-602.
- White R.W. and Powell R., 2002. Melt loss and the preservation of granulite facies mineral assemblages. *Journal of Metamorphic Geology* 20, 621-632.
- White R.W., Powell R., Clarke G.L., 2002. The interpretation of reaction textures in Fe-rich metapelitic granulites of the Musgrave Block, central Australia: Constraints from mineral equilibria calculations in the system K_2O - FeO - MgO - Al_2O_3 - SiO_2 - H_2O - TiO_2 - Fe_2O_3 . *Journal of Metamorphic Geology* 20, 41-55.
- White R.W., Powell R., Holland T.J.B., 2007. Progress relating to calculation of partial melting equilibria for metapelites. *Journal of Metamorphic Geology* 25, 511-527.
- Whitney D.L. and Irving A.J., 1994. Origin of K-poor leucosomes in a metasedimentary migmatite complex by ultrametamorphism, syn-metamorphic magmatism and subsolidus processes. *Lithos* 32, 173-192.
- Winkler H.G.F., 1976. *Petrogenesis of Metamorphic Rocks*, 4th Edition, Springer-Verlag, New York.
- Xu Cheng., Huang Z., Qi L., Fu P., Liu C., Li E., Guan T., 2007. Geochemistry of cretaceous granites from Mianning in the Panxi region, Sichuan Province southwest china: Implications for their generation. *Journal of Asian Earth Sciences* 29, 737-750.
- Xu L.J., Liu S.A., Wang Z.Z., Liu C., Li S., 2019. Zinc isotopic compositions of migmatites and granitoids from the Dabie Orogen, central China: Implications for zinc isotopic fractionation during differentiation of the continental crust. *Lithos* 324-325, 454-465.
- Zhang H., Li S.Q., Fang B.W., He J.F., Xue Y.Y., Siebel W., Chen F., 2018. Zircon U-Pb ages and geochemistry of migmatites and granites in the Foping dome: Evidence for Late Triassic crustal evolution in South Qinling, China. *Lithos* 296-299, 129-141.
- Zuluaga C.A., Amaya S., Uruena C., Bernet M., 2017. Migmatization and low-pressure overprinting metamorphism as record of two pre-Cretaceous tectonic episodes in the Santander Massif of the Andean basement in northern Colombia (NW South America). *Lithos* 274-275, 123-146.



This work is licensed under a Creative Commons Attribution 4.0 International License CC BY. To view a copy of this license, visit <http://creativecommons.org/licenses/by/4.0/>

